CONSTRAINING 3-D ERT WITH GPR REFLECTION DATA

Journal of Applied Geophysics:

Doetsch, J., Linde, N., Pessognelli, M., Green, A. G., and Günther, T., 2011. Constraining 3-D electrical resistance tomography with GPR reflection data for improved aquifer characterization, *Journal of Applied Geophysics*, *78*. 68-76.

ABSTRACT

Surface-based ground penetrating radar (GPR) and electrical resistance tomography (ERT) are common tools for aquifer characterization, because both methods provide data that are sensitive to hydrogeologically relevant quantities. To retrieve bulk subsurface properties at high resolution, we suggest incorporating structural information derived from GPR reflection data when inverting surface ERT data. This reduces resolution limitations, which might hinder quantitative interpretations. Surface-based GPR reflection and ERT data have been recorded on an exposed gravel bar within a restored section of a previously channelized river in northeastern Switzerland to characterize an underlying gravel aquifer. The GPR reflection data acquired over an area of 240×40 m map the aquifer's thickness and two internal sub-horizontal regions with different depositional patterns. The interface between these two regions and the boundary of the aquifer with the underlying clay are incorporated in an unstructured ERT mesh. Subsequent inversions are performed without applying smoothness constraints across these boundaries. Inversion models obtained by using these structural constraints contain subtle resistivity variations within the aquifer that are hardly visible in standard inversion models as a result of strong vertical smearing in the latter. In the upper aquifer region, with high GPR coherency and horizontal layering, the resistivity is moderately high (>300 Ωm). We suggest that this region consists of sediments that were rearranged during more than a century of channelized flow. In the lower low coherency region, the GPR image reveals fluvial features (e.g., foresets) and generally more heterogeneous deposits. In this region, the resistivity is lower (~200 Ωm), which we attribute to increased amounts of fines in some of the well-sorted fluvial deposits. We also find elongated conductive anomalies that correspond to the location of river embankments that were removed in 2002.

1.1 INTRODUCTION

Near-surface geophysical techniques can be useful in a wide range of hydrogeological applications [*Rubin and Hubbard*, 2005; *Hubbard and Linde*, 2011]. Surface-based ground penetrating radar (GPR) and electrical resistance tomography (ERT) are perhaps the most common geophysical methods used, primarily because of the hydrogeological relevance of the respective physical properties and their relative ease of application along profiles ranging from 1 to 10,000 m and surface areas ranging from 1 to 10,000 m^2. Electrical resistivity in saturated alluvial systems is mostly a function of pore-water salinity, porosity, tortuosity and

the specific surface area of the grains (i.e., the amount of fine materials) [*Lesmes and Friedman*, 2005]. Unfortunately, surface-based ERT suffers from resolution limitations [*Ellis and Oldenburg*, 1994] that enhance the inherent non-uniqueness of the resistivity inverse problem [*Parker*, 1984]. In contrast, GPR reflection data can, under favorable conditions (e.g., for soil and sediments with low clay content and only moderate pore-water salinity), be used to map the 3-D sedimentary structure of the subsurface in great detail down to about 10 m depth [*Smith and Jol*, 1992; *Beres et al.*, 1995; *Beres et al.*, 1999; *Lunt et al.*, 2004]. Since GPR reflections are mainly sensitive to contrasts in water content, it is often difficult to relate GPR images to the bulk properties of a hydrogeological model. We propose here to incorporate structural information derived from surface GPR reflection data as constraints in the inversion of surface ERT data that provides such bulk properties.

The sedimentary structures of fluvial deposits have been extensively studied using GPR reflection imaging [e.g., *Smith and Jol*, 1992; *Huggenberger*, 1993; *Beres et al.*, 1995; *Beres et al.*, 1999]. For example, *Lunt et al.* [2004] used GPR measurements to develop a model for the evolution of gravelly braided bars. Surface-based ERT has also been widely used for aquifer characterization [e.g., *Kosinski and Kelly*, 1981; *Mazac et al.*, 1987; *Koch et al.*, 2009]. In a number of studies, surface-based GPR reflection and ERT methods have been combined to improve the characterization of alluvial aquifers [e.g., *Sandberg et al.*, 2002; *Bowling et al.*, 2005; *Bowling et al.*, 2007; *Bélanger et al.*, 2010].

Integration of different geophysical data or models for interpretation purposes can be achieved by the (1) joint interpretation of results from separately processed / inverted data, (2) joint inversion of different data sets and (3) constrained inversion of one data set using information from other geophysical data / models. Joint interpretation of different models is common practice [e.g., *Sandberg et al.*, 2002; *Bowling et al.*, 2005; *Bélanger et al.*, 2010], but becomes ambiguous when the models disagree or their resolution properties differ significantly. These problems can be partly avoided by performing joint inversion, which is becoming increasingly used since the development of structural joint inversion [*Haber and Oldenburg*, 1997; *Gallardo and Meju*, 2003]. In crosshole configurations, joint inversion of GPR traveltimes and ERT has been used for aquifer characterization [e.g., *Linde et al.*, 2006a] to provide higher resolution and geometrically similar models that can be used to estimate effective petrophysical parameters (see Chapter 2). Constrained inversion is particularly useful when one wants to combine geophysical data that are mainly sensitive to structure (e.g., seismic and GPR reflection data) with data that are primarily sensitive to bulk properties

(e.g., ERT data). As examples, *Favetto et al.* [2007], *Jegen et al.* [2009] and *Li et al.* [2003] improved the inversion results of gravity and magnetotelluric data by constraining the inversions using interfaces defined in seismic reflection models.

Here, we investigate the extent to which GPR-derived interfaces can improve ERT inversion and subsequent aquifer characterization. The constraints are implemented by conditioning an unstructured inversion mesh to these interfaces and by not imposing any smoothness constraints across these interfaces during the inversion. An unstructured mesh is essential to include surface topography [*Günther et al.*, 2006], arbitrary electrode positions and prior structural information.

We test our methodology (see Figure 5.1 for a flow chart) on data acquired on a gravel bar within a restored section of the Thur River channel in northeastern Switzerland (see inset in Figure 5.2). The primary goals of this study are to (1) map the geometry of the gravel aquifer on the scale of the gravel bar, (2) resolve the sedimentary structure of the aquifer, and (3) determine if any evidence of the old river embankment remains. Other researchers working at the site will use this information and it will serve as a basis for a saline tracer experiment to be monitored with ERT. After introducing our field site, we describe the GPR acquisition and processing, followed by ERT acquisition and inversion, and a joint interpretation of the resulting models.

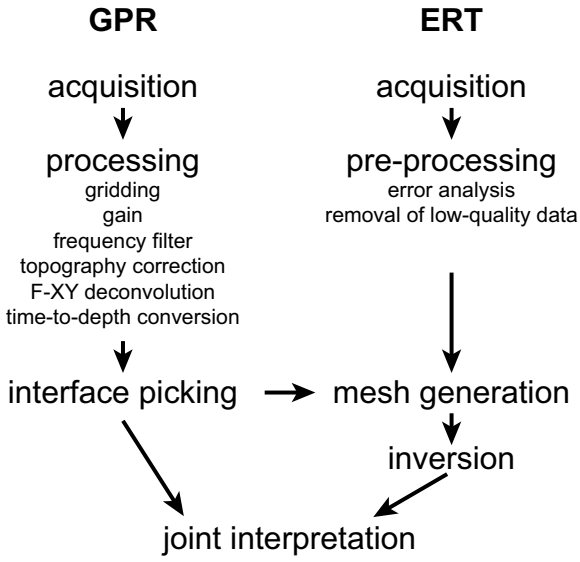

Figure 5.1. Work flow for the combined processing of 3-D GPR and ERT data. The GPR processing is fully independent, but the ERT mesh generation, regularization, and thus the subsequent inversion results are strongly influenced by the GPR-mapped interfaces.

1.2 THUR RIVER FIELD SITE

The Thur River is the largest Swiss river without natural or artificial reservoirs. It is a peri-alpine tributary of the Rhine River with a catchment area of ~1750 km^2. Water level and discharge variations in the Thur River are similar to those of unregulated alpine rivers. Like many other rivers, the meandering Thur River was channelized towards the end of the 19th century for flood protection and to gain arable land. In an attempt to combine flood protection with ecological objectives, a more natural environment was restored along a 2.5 km long reach of the Thur, starting in 2002. The effects of this restoration effort are currently being investigated within the RECORD project [for details see *RECORD*, 2011; *Schneider et al.*, 2011].

While the channelized river was practically flowing along a straight course prior to restoration (Figure 5.2a), the river bed morphology changed substantially once the northern embankment and overbanks were removed. By 2005, a gravel bar had developed on the northern shore of the river (Figure 5.2b) with a surface exposure that strongly depends on the varying river discharge. Under low flow conditions (20 m^3/s), a low-lying region with clean gravel is exposed at the surface, whereas under intermediate flow conditions (100 m^3/s), this region is flooded and the gravel bar consists mainly of grass-colonized gravel. Under high-flow conditions (200 m^3/s), the entire gravel bar is flooded. The frequent flooding of large parts of the gravel bar and the resulting movement of sediments precludes permanent installations, such as monitored boreholes, and thereby increases the importance of geophysics for site characterization. The GPR and ERT data were acquired at low flow conditions. The aquifer below consists of highly permeable fluvial gravel deposits with a varying fraction of fine material.

Ten boreholes instrumented with loggers (temperature, electrical conductivity and pressure) were located on the upper regions of the gravel bar to investigate river-groundwater interactions at the site [*Vogt et al.*, 2010b; *Vogt et al.*; *Schneider et al.*, 2011]. The GPR and ERT data presented here were acquired on the gravel bar to delineate the subsurface aquifer structure for future hydrogeological studies. The surveys were designed to cover as much of the gravel bar as possible; the GPR survey area was limited to the areas of open and grass-colonized gravel, whereas the ERT measurements also covered the Salix-populated northern part of the gravel bar (Figure 5.2). The coordinate system used in this paper has its origin at Swiss grid coordinates 272036 / 700218 and is rotated 17° counterclockwise to align the *x*-axis with the river flow direction.

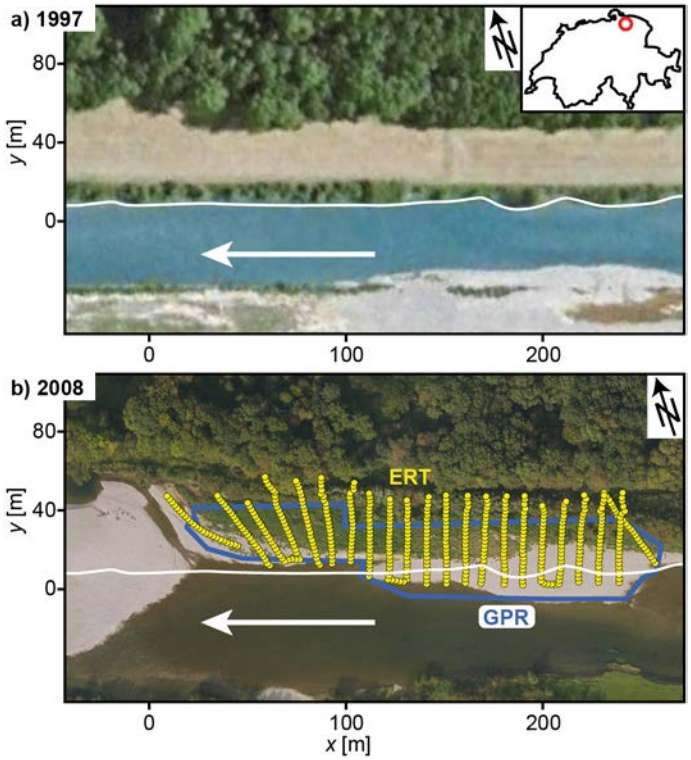

Figure 5.2. Aerial photographs of the Thur River (northeastern Switzerland) (a) before and (b) after restoration. Since the river restoration in 2002, the river bed morphology has been rapidly changing. For reference, the location of the 1997 embankment (shoreline) is highlighted in both photos (white line) and the river flow direction is indicated by a white arrow. Overlain on the 2008 image are the ERT electrode positions and the extent of the 3-D GPR surveys.

1.3 GPR DATA ACQUISITION, PROCESSING AND INTERPRETATION

1.3.1 Data acquisition

The GPR data were acquired in March 2008 (western part at $x < 100$ m in Figure 5.2b) and January 2009 (eastern part at $x > 100$ m). A 100 MHz PulsEkko Pro system was used to collect traces semi-continuously with an internal stacking of 8 and a trace length of 320 ns (trace interval of ~5 cm). The measurements were time stamped using a static GPS receiver. An additional mobile GPS receiver attached to the antenna sledge was used to record accurate midpoint positions using differential processing [*Streich et al.*, 2006]. Densely spaced lines (line spacing of 0.5 m) acquired parallel to the river were used to cover the gravel bar. Because the resulting data set had limited crossline resolution, eight complementary 2-D lines were recorded perpendicular to the river. These lines were important to avoid spatial aliasing on the crosslines extracted from the 3-D data.

In addition to the common-offset measurements, 12 common-midpoint (CMP) measurements were made at 9 different positions to determine velocities and velocity variations within the survey area. A representative CMP is presented in Figure 5.3.

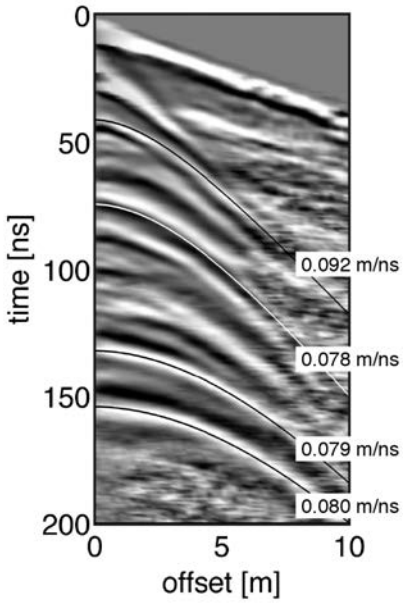

Figure 5.3. Representative common-midpoint (CMP) gather for GPR velocity determination from a high-lying point on the gravel bar.

1.3.2 Processing

Pre-processing of all traces included dewow filtering, alignment of zero times and coordinate assignment based on the differential GPS data. The coordinate assignment was achieved by matching the GPS times of each trace with the time stamps of the GPS attached to the acquisition sledge. The total number of acquired traces for the 3-D surveys was 111,291 (2008) and 245,130 (2009). These traces were summed within regular 0.2 m (in-line) by 0.5 m (crossline) bins. To obtain the best gridding result for the uneven trace spacing, we adapted the natural neighbor gridding algorithm of *Sambridge et al.* [1995]. The two gridded data volumes had a spatial extent of 80 × 25 m (2008) and 160 × 36 m (2009) and together covered the full gravel bar over a length of 240 m (Figure 5.2b).

Further data processing included application of a gain function, frequency filtering, topography correction and F-XY deconvolution. The gain function was based on a smoothed inverse of the Hilbert transform of the data with a maximum gain set to 500. The frequency bandpass filter around a center frequency of 80 MHz was cosine tapered with corner frequencies of 15-45-115-145 MHz. In the next step, the data were corrected for topography

using the elevation data obtained from the differential GPS measurements. We used a velocity of 0.09 m/ns for the topography correction (based on the CMP results for the unsaturated gravel; see Figure 5.3). Topography correction and F-XY deconvolution were carried out using commercial software, whereas in-house MATLAB® routines were used for the other processing steps. The F-XY deconvolution suppressed laterally incoherent signal and improved the images of coherent features. Migration was not necessary, because the steepest dips observed in the data were <20°. Migration tests confirmed this assertion and showed that migration decreased the signal quality in some areas due to the different in-line and crossline trace spacings.

For interpretation, the vertical axis was converted from time to depth using a two-layer velocity model that represented the unsaturated and saturated gravel. The velocity estimates, based on the analysis of the 12 CMP measurements, were $v_u = 0.09$ m/ns ± 10% for the unsaturated gravel and $v_w = 0.075$ m/ns ± 10% for the saturated gravel.

1.3.3 GPR interpretation

Figure 5.4 shows a chair plot of the western part of the GPR data volume together with a photograph of fluvial deposits at a gravel pit 10 km from the survey area. The data quality is generally very high within the gravel aquifer, such that coherent reflections can be traced to 5 - 6 m depth. At this level, reflections originate from the boundary between the gravel aquifer and underlying lacustrine clay aquitard (marked in Figure 5.4b).

The GPR image (Figure 5.4b) provides many details about the fluvial deposits. These images are comparable with those obtained across nearby gravel deposits [e.g., *Huggenberger*, 1993; *Beres et al.*, 1995; *Beres et al.*, 1999]. Regions with well-sorted gravels, such as the foresets FO in Figure 5.4b (see also FO' in Figure 5.4a), can be distinguished from sub-horizontal features (GS and GS') that were deposited in a different flow regime. Based on Figure 5.4a, it seems likely that these different depositional units have different hydrogeological properties [*Beres et al.*, 1995; *Beres et al.*, 1999]. The foresets (FO and FO') consist of a sequence of open framework gravel and units with a bimodal grain size distribution. The clean gravel zones are expected to have a very high hydraulic conductivity, such that the controlling factor for determining the hydraulic conductivity in this region is the connectivity of these small gravel sub-units. In contrast, the gravel sheets (GS and GS') have a much larger extent, a wider grain size distribution and are poorly sorted. It is expected that the

hydraulic conductivity distribution in the gravel sheets is less heterogeneous than in the foresets [e.g., *Heinz et al.*, 2003].

The same depositional units can be identified in the full GPR volume displayed in Figure 5.5a and b. Three different units are separated by two interfaces that appear as continuous reflections in the GPR image. The lower interface is the gravel-clay boundary, whereas the upper interface separates the different depositional structures (FO and GS in Figure 5.4b) of the gravel aquifer. The two main interfaces were semi-automatically picked throughout the GPR volume (Figure 5.5b) using commercial interpretation software. Simultaneous display of in-line and crossline sections with associated picks allowed consistent 3-D picking. These interfaces were extrapolated short distances outside the GPR survey area for the ERT mesh generation (see Figure 5.2b).

Differences between the two regions of the aquifer are highlighted in the coherency plot of Figure 5.5c. The coherency of the GPR data was calculated using a moving cell [*McClymont et al.*, 2008] with a side-length of 2.5 m in the horizontal and 0.5 m in the vertical direction, with a maximum assumed dip of 20°. The coherency is highest in the upper part of the aquifer with the predominantly horizontal layering and is much reduced in the lower part. This strong horizontal layering is restricted to the region underlying the river channel prior to restoration (Figure 5.2a). Below the region of this pre-restoration channel, the top 3 m of the aquifer are strongly layered (Figure 5.6a), which is not observed outside this region (Figure 5.6b and c). Figure 5.6a also shows a channel-like feature (SC) that corresponds to the location of a side channel mapped in 1811 (Amt für Geoinformatik des Kantons Thurgau, personal communication).

1.4 ERT DATA ACQUISITION AND INVERSION

1.4.1 Acquisition and pre-processing

ERT data covering the entire gravel bar were acquired over a period of two days in March 2009. To survey the full gravel bar, we employed a 3-D roll-along scheme with a total of 22 quasi-parallel lines perpendicular to the river (Figure 5.2b). A total of 528 electrode positions were used, with an electrode spacing of 2 m along the lines and a line separation of ~8 m. Three-dimensional measurements were made on patches covered by electrodes from 6 of the parallel lines. This setup was then moved by 4 lines to have an overlap of 2 lines between the patches (5 of these patches covered the gravel bar). Within each of the patches, dipole-dipole,

equatorial dipole, Wenner and gradient data sets (for details of these configurations, see [*Zonge et al.*, 2005]) were collected both along and across the quasi-parallel lines. The quality of the 35,514 raw measurements was evaluated on the basis of the stacking errors (4-6 stacks) and by comparing the repeated measurements associated with overlapping patches. The data set was reduced by combining the repeated measurements, deleting poor-quality data and removing data with geometrical factors >1000 to yield a final data set of 16,349 values. Most of the eliminated data were not included in the design of the measurement sequence, but were added to optimize the recording on the 10-channel SyscalPro instrument. We included these measurements in the initial processing, but had to remove most of them due to their unfavorable electrode geometry. An overall error level of 3% (estimated from the repeated measurements) was added to the standard deviations estimated from the stacking process; these error estimates were used in the inversions.

The horizontal and vertical positions of the electrodes were measured with a differential GPS system and surface topography was estimated using linear interpolation between the electrode positions.

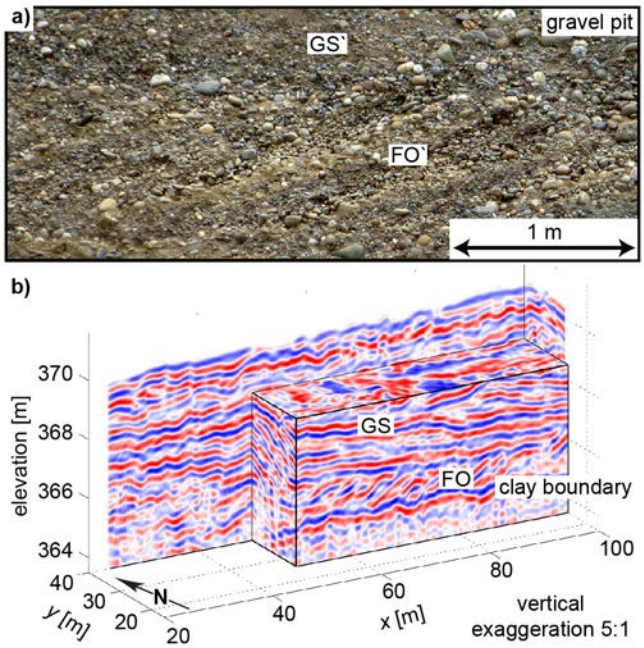

Figure 5.4. (a) Photo of fluvial deposits at a gravel pit (located 10 km away from the survey area) and (b) chair plot of the GPR results for the western (downstream) end of the gravel bar. Foresets (FO in (b) and FO` in (a)) and the subhorizontal layering (GS in (b) and GS` in (a)) illustrate the different sedimentation types of the fluvial system. The strong reflection at 5 - 6 m depth marks the interface between the gravel aquifer and the underlying clay aquitard.

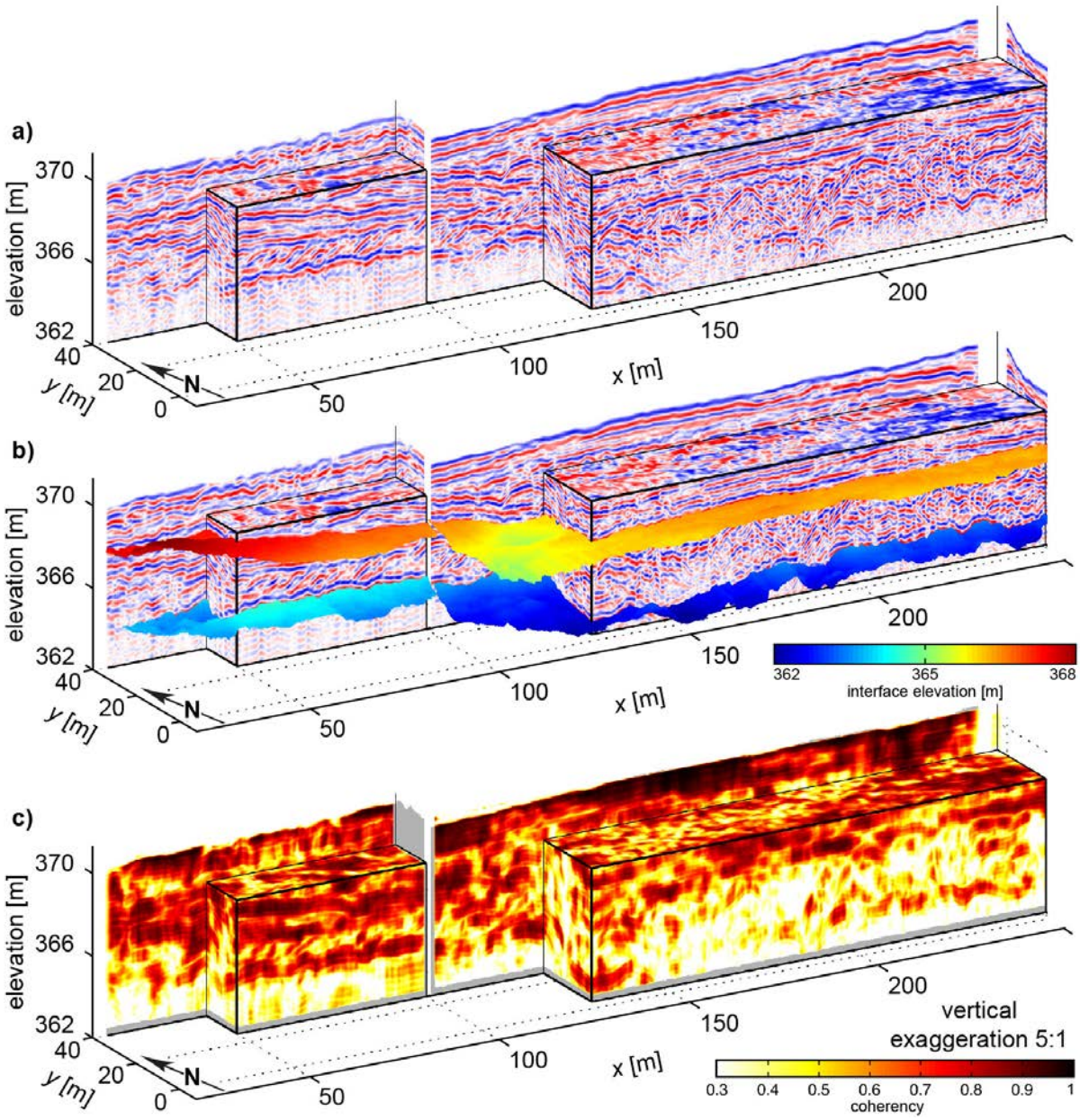

Figure 5.5. GPR results for the entire gravel bar. (a) Chair plot of the fully processed and depth converted data. (b) As in (a), but including the picked interfaces within the GPR volume. (c) Coherency of the GPR signal based on a coherency analysis. The signal coherency is much decreased in the lower part of the gravel aquifer at $x > 150$ m.

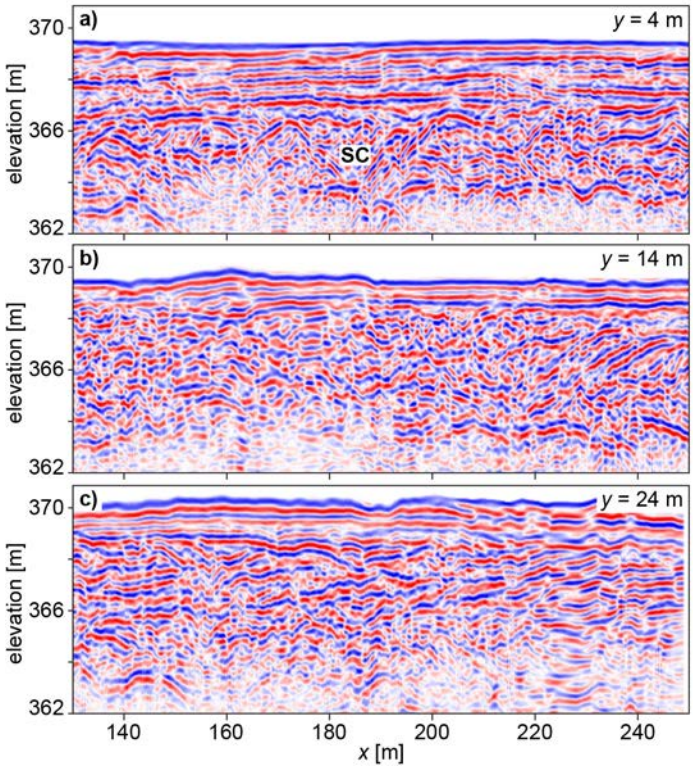

Figure 5.6. Vertical cuts through the GPR volume, parallel to the *x*-axis at a) *y* = 4m (corresponding to one of the cuts in Figure 5), (b) 14 m and (c) 24 m. One can observe a clear difference in the depositional pattern in the top 3 m of the aquifer between (a) the pre-restoration river channel and (b) and (c) the outside regions that never experienced channelized river flow. SC marks a channel-like feature, which corresponds to the location of a side channel mapped in 1811.

1.4.2 Mesh generation

The mesh or grid that represents the models plays a critical role in 3-D ERT inversion [*Günther et al.*, 2006]. We use an unstructured tetrahedral mesh that allows us to include arbitrary electrode positions, surface topography and such additional structural information as the water table and GPR-defined interfaces.

The gridding was performed in two steps: (1) mesh the 2-D surfaces and (2) create a 3-D tetrahedral mesh based on the 2-D meshes. In the first step, the 2-D surfaces were represented by a mesh of triangles that included the electrode positions as points. The water table was assumed to be constant at the measured elevation of 371.2 m (the hydraulic gradient is very low due to the high permeability of the aquifer [*Vogt et al.*, 2010b]) and the interfaces within and at the base of the gravel aquifer were interpolated from the horizons shown in Figure 5.5b.

In the second step, the 2-D grids were used as a starting point for the 3-D tetrahedral mesh generation [*Rücker et al.*, 2006]. Three different meshes were created (see Figure 5.7a, c

and e) to evaluate the effects of the GPR-defined structural constraints on the ERT results. The first mesh (Figure 5.7a) only included the surface topography, whereas the second mesh (Figure 5.7c) also included the water table and the gravel-clay boundary, and the third mesh (Figure 5.7e) included all of these interfaces together with the GPR-defined interface within the gravel aquifer. Regions above and below intra-gravel and gravel clay interfaces were treated as separate regions during the inversion (i.e., no smoothing constraints were applied across the interfaces). By comparison, the water table was included in the meshing, but the unsaturated zone was not decoupled from the layer below during the inversion. Each of the three inversion meshes had approximately 100,000 cells and a 270 × 80 × 25 m extent.

For the forward calculations, the inversion mesh was refined by splitting each tetrahedron into eight. The modeling domain was extended 30 m in all directions to reduce boundary effects. The singularity removal technique of Lowry et al. [1989] was used to achieve high accuracy by accounting for the rapid decay of electric potential around each current-source position [*Rücker et al.*, 2006]. Since there is no analytical solution for the primary potentials in the presence of topography, the potential field (for a homogeneous earth) was calculated using a refined mesh around the electrodes before the inversion. For the forward calculations, Neumann (no current flow) boundary conditions were used at the surface and mixed-type boundary conditions were used along the other sides of the mesh [*Rücker et al.*, 2006].

1.4.3 ERT inversion

For each of the three meshes described above, the ERT data were inverted using the electrical resistance tomography program BERT of *Günther et al.* [2006]. The starting models had a homogeneous resistivity of 200 Ωm in the aquifer and 40 Ωm in the clay (for the meshes in Figure 5.7c and e). Tests using uniform resistivities of 20 Ωm, 200 Ωm and 500 Ωm throughout the models showed that the features in the aquifer were well-resolved and that the resistivity of the clay layer varies only moderately between 35 Ωm and 55 Ωm, depending on the starting model. An anisotropy factor of 0.5 was assumed for the smoothness constraints within the aquifer to honor the layered structure imaged by the GPR (for the formulation of these constraints, see *Coscia et al.,* [2011a]). The data were first inverted using the three-region mesh (Figure 5.7e) and the inversion algorithm was allowed to slightly adapt the error model by robust data reweighting [*Claerbout and Muir*, 1973] from a median of 3.0% to 3.5%. The final error estimates from this inversion were then assigned to each data point and the data were inverted to this error level for all three meshes.

For each of the three meshes, the data were inverted using seven different regularization weights ranging from λ=20 to λ=300. For the interpretation, we chose the model with the strongest regularization that explained the data to the specified error model. Inversions using the two- and three-layer meshes (Figure 5.7c and e) reached the data misfit criterion (normalized RMS = 1) in 6 and 5 iterations using a regularization weight of λ=70 and λ=100 [*Günther et al.*, 2006], respectively. The lowest data misfit for the standard inversion without any interface decoupling was obtained using λ=50, but the final normalized RMS after 9 iterations was 1.3 times the assumed data error, with no improvement after additional iterations. The three resulting models are shown in Figures 5.7b, d, f and 5.8 (in this latter figure, the ERT models are shown in the same view and with the same vertical exaggeration (5:1) as the GPR images in Figure 5.5).

Although the inversion parameters are comparable and the three models with roughly the same number of cells fit the data to approximately the same error level, the inversion results (especially at depth) are very different. These results illustrate the inherent limitations of ERT data to determine uniquely subsurface structure with depth [e.g., *Parker*, 1984]. Standard ERT that only includes surface topography as a structural constraint yields a vertically and horizontally smooth model (Figure 5.7b). Such smoothness is an inherent feature of Occam-type inversions that may hinder interpretations of the models [*Ellis and Oldenburg*, 1994]. It is possible to identify the low-resistivity clay, as well as the high-resistivity aquifer in Figure 5.7b, but it is difficult to discern a clear boundary between the two layers and interpret features within the aquifer. In the model obtained using the mesh that includes the water table and the gravel-clay boundary (Figure 5.7d), it is possible to differentiate clearly between the gravel aquifer and the clay, thereby creating an image that better matches our prior knowledge. Two effects contribute to the differences between the models in Figure 5.7b and d. First, by including the gravel-clay boundary in the meshing, there are no cells that are partly located in the gravel and partly in the clay, thus allowing the inversion algorithm to define a much sharper boundary. This effect is enhanced by the relatively coarse model discretization of the aquifer, which is a consequence of computational limitations when inverting large-scale 3-D ERT data sets. Second, disconnecting the regularization above and below this interface allows the discrete jump in resistivity from ~200 Ωm (gravel) to ~30 Ωm (clay). This is implemented by neglecting cells across the defined interfaces in the roughness operator that penalizes changes between neighboring cells [*Günther and Rücker*, 2006]. Varying the interface depth within the uncertainty range of ±10% slightly changed the

resistivity model in the vicinity of the interfaces, but did not change the features discussed in the interpretation.

Including the interface within the gravel layer (Figures 5.7e, f and 5.8c) makes it possible to resolve better the resistivity variations within the aquifer that are only hinted at in Figures 5.7d and 5.8b. The model clearly shows that the aquifer at the position marked with A in Figure 5.8c is divided into two zones of distinctly different resistivity. Whereas Figure 5.8b shows resistivities of ~300 Ωm in this region, Figure 5.8c indicates resistivities of ~400 Ωm above and ~200 Ωm below the interface, although both models fit the data to the same error level.

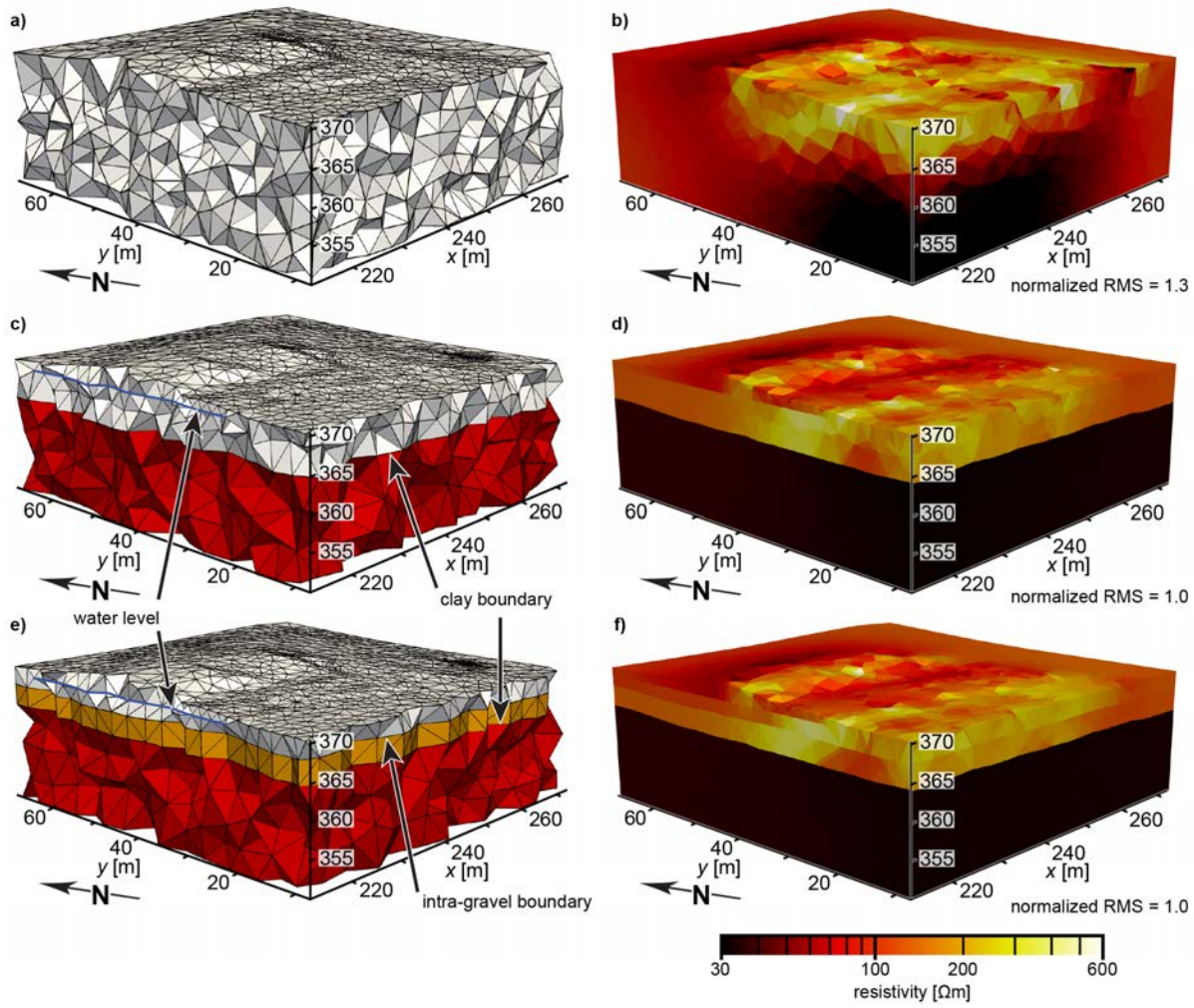

Figure 5.7. Part of the ERT inversion (parameter) mesh for the cases with (a) no interfaces (standard inversion), (c) including the gravel - clay boundary and (e) additionally including the interface within the gravel. Note, that (c) and (e) also incorporate the water table, but without layer decoupling (see text). All three meshes have approximately the same number of cells. (b), (d) and (f) Inversion models for the parts of the three meshes shown in (a), (c) and (e), respectively. More details are visible in (d) and (f), due to reduced vertical smearing over known interfaces.

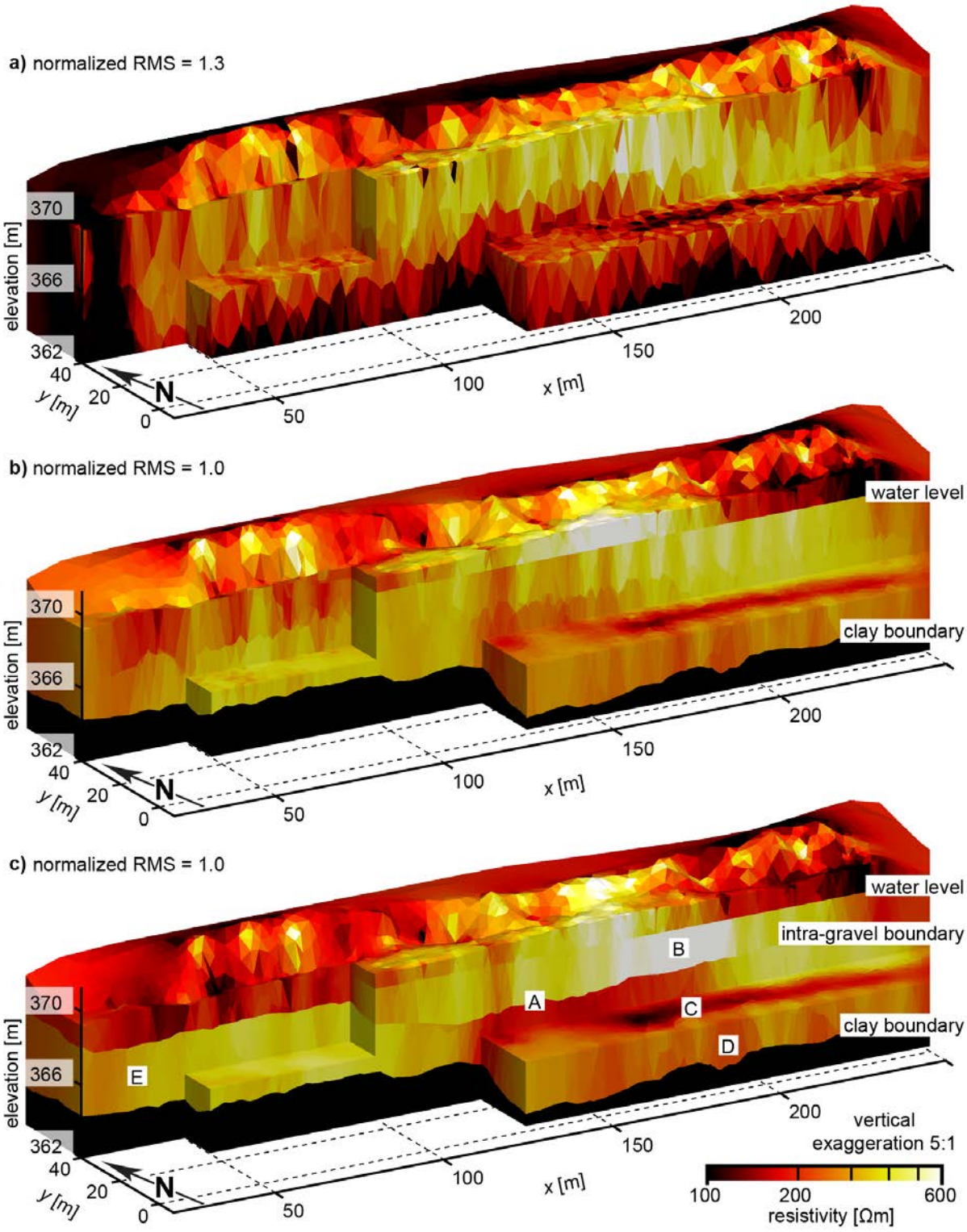

Figure 5.8. ERT models obtained using the inversion meshes shown in (a) Figure 5.7a, (b) Figure 5.7c and (c) Figure 5.7e. The view is the same as in Figure 5.5. Note that the colour scale is saturated at 100 Ωm to focus on the resistivity variations within the aquifer. The deepest layer in (b) and (c) has a resistivity of $\rho \sim 30$ Ωm. For a discussion of A-E, see text.

1.5 INTERPRETATION AND DISCUSSION

We know from the piezometer installations that the gravel aquifer is underlain by a thick clay aquitard at 5 - 6 m depth [*Vogt et al.*, 2010b]. Our GPR data have allowed us to map this interface throughout the surveyed part of the aquifer (Figure 5.5b). However, depth errors occur as a consequence of the constant GPR velocity model assumed for the aquifer. Velocities within the aquifer vary by about ±10% according to the CMP analyses and crosshole GPR measurements at a neighboring site (Chapter 2), which leads to corresponding relative depth errors in the same range. The aquifer is thickest in the middle of the gravel bar, becoming thinner in the western ($x < 100$ m) part. The interface within the gravel is relatively flat in the eastern ($x > 150$ m) part, deepening towards the middle and approaching the surface at the western end.

The ERT model obtained by incorporating all interfaces in the inversion (Figure 5.8c) allows us to interpret resistivity variations within the aquifer, which is hardly possible otherwise (Figure 5.8a and b). Resistivities in the unsaturated zone are largely controlled by the soil cover. We interpret high resistivities ($\rho > 500$ Ωm) as indicative of unsaturated relatively clean gravels and low resistivities (as low as 60 Ωm) as sandy loam. The relatively high resistivity of $\rho > 400$ Ωm in the upper part of the aquifer at B in Figure 5.8c indicates clean gravel with a relatively low porosity of ~20% (Chapter 2). We suspect that this region of the aquifer comprises sediments deposited after channelization of the river. This hypothesis is supported by the GPR data, which maps strong horizontal layering in this region and a lateral change towards more heterogeneous depositional patterns from the old river embankment (Figure 5.2a) towards the north (Figure 5.6). Low resistivities coincide with the old river embankments (C in Figure 5.8c). The source of these low resistivities is unclear, but they may be due to an increased deposition of fines during the period of channelized flow, which may mean that the restored site still has an unnatural flow barrier with implications for hyporheic processes.

The resistivities and GPR coherencies vary in the lower part of the aquifer (Figure 5.8c). Low resistivities (~200 Ωm) indicating higher porosities and higher clay content are found at the eastern ($x > 150$ m) end (D in Figure 5.8c), whereas intermediate resistivities (~300 Ωm) are seen at the western end (E in Figure 5.8c). Although these features can be seen in Figure 5.8b, they are imaged more clearly in Figure 5.8c. The low resistivities coincide with low GPR coherency, whereas intermediate and high resistivities coincide with high GPR coherency (compare Figures 5.5c and 5.8c). We interpret regions of high resistivity and high

coherency as clean gravel with strong horizontal layering and low resistivity and low coherency within the aquifer in terms of more heterogeneous deposits consisting of sequences of fine and coarse sediments. The low resistivities are mainly caused by the fine materials found in some of the lower sub-units [*Heinz et al.*, 2003]. We suggest that this region consists of sediments that were deposited before the channelization of the river.

The two regions of the gravel aquifer with differing reflection patterns and resistivity are likely to have different hydrogeological properties. The upper part is expected to be less heterogeneous and to have intermediate hydraulic conductivities compared to the end members of the more heterogeneous units in the deeper part [*Heinz et al.*, 2003]. Even though a quantitative hydrogeological interpretation is not feasible at this stage, our models are useful for developing a conceptual hydrogeological model. We plan to investigate groundwater flow patterns at the site by performing a saline tracer test to be monitored with 3-D ERT.

One important challenge in hydrogeophysics is to create quantitative hydrogeological models at high resolution on scales that are larger than the 5-10 m borehole separation typically employed in quantitative hydrogeophysical studies [*Hubbard and Linde*, 2011]. We find that the estimated range of resistivities in the aquifer is very similar to those obtained using crosshole ERT within a suite of boreholes located 15 km upstream adjacent to an unrestored section of the river [Chapters 2 and 4; *Coscia et al.*, 2011a]. Since the depositional environments are very similar at the two sites, it is possible that any field-scale relationship between resistivity and porosity/hydraulic conductivity established at the unrestored upstream site could be applicable at the restored site, but for a model volume that is 10-100 times larger.

It appears that the combination of joint inversions of smaller scale crosshole data (Chapter 2) with constrained inversions of larger scale surface-based data is a promising approach for improving the information content extracted from surface-based geophysical data at intermediate scales. The combination of at least two complementary geophysical data types is important. Consider the lower conductive part of the aquifer in the eastern area. The GPR image supplies details on the heterogeneous sedimentary units, whereas the ERT model provides upscaled effective bulk properties.

1.6 CONCLUSIONS

We have acquired surface-based 3-D GPR reflection and ERT data to characterize an alluvial aquifer underlying a gravel bar at a restored river section. The GPR data imaged undulations in the thickness of the aquifer and delineated two layers in the aquifer with different reflection patterns. Whereas the upper part of the gravel aquifer appeared to be only weakly heterogeneous and displays subhorizontal layering, the deeper part is moderately heterogeneous and displays complex fluvial features. By including GPR reflection interfaces corresponding to the base and internal layers of the aquifer in the ERT mesh and by disconnecting the regularization across these interfaces, we were able to improve markedly the resulting ERT models. The standard and constrained inversion results illustrated to what extent ERT data constrain features, particularly at depth, and how important it is to (wherever possible) perform constrained inversions to obtain quantitative information on resistivity structure and properties. Models that incorporated the GPR interfaces revealed resistivity variations within the aquifer that were not resolved in the unconstrained model.

The final GPR-constrained ERT model has moderate resistivities in the upper part of the aquifer indicating rather low porosities and negligible clay content. In the same region, the GPR coherency is very high. In the lower part of the aquifer, the electrical resistivity is significantly lower with values decreasing in the *x*–direction. The GPR coherency shows a remarkably similar pattern.

The lower part of the aquifer is expected to have a highly variable hydraulic conductivity. The magnitude of the upscaled conductivity in this zone is likely to be dependent on the connectivity of the more permeable deposits. With respect to river restoration, we suggest that the upper part of the aquifer consists of gravel sheets that were probably rearranged by the river as a result of channelization at the end of the 19th century. Furthermore, we find that a low-resistivity feature, probably indicating enhanced clay-content, coincides with the location of the former river embankment. Regardless of origin, it appears that 100 years of a channelized flow regime has had a strong and persistent influence on the aquifer structure.

REFERENCES

Acworth, R. I., and Dasey, G. R., 2003. Mapping of the hyporheic zone around a tidal creek using a combination of borehole logging, borehole electrical tomography and cross-creek electrical imaging, New South Wales, Australia, *Hydrogeology Journal*, **11**, 368-377.

Ajo-Franklin, J. B., Minsley, B. J., and Daley, T. M., 2007. Applying compactness constraints to differential traveltime tomography, *Geophysics*, **72**, R67-R75.

al Hagrey, S. A., and Müller, C., 2000. GPR study of pore water content and salinity in sand, *Geophysical Prospecting*, **48**, 63-85.

Allègre, V., Jouniaux, L., Lehmann, F., and Sailhac, P., 2010. Streaming potential dependence on water-content in Fontainebleau sand, *Geophysical Journal International*, **182**, 1248-1266.

Alumbaugh, D., Chang, P. Y., Paprocki, L., Brainard, J. R., Glass, R. J., and Rautman, C. A., 2002. Estimating moisture contents in the vadose zone using cross-borehole ground penetrating radar: A study of accuracy and repeatability, *Water Resources Research*, **38**, 1309.

Alumbaugh, D. L., and Newman, G. A., 2000. Image appraisal for 2-D and 3-D electromagnetic inversion, *Geophysics*, **65**, 1455-1467.

Annan, A. P., 2005. GPR Methods for Hydrogeological Studies, in *Hydrogeophysics*, edited by Y. Rubin and S. S. Hubbard, pp. 185-213, Springer Netherlands.

Archie, G. E., 1942. The electrical resistivity log as an aid in determining some reservoir characteristics, *Transactions of the American institute of Mining, Metallurgical and Petroleum Engineers*, **146**, 54-62.

Arora, T., Linde, N., Revil, A., and Castermant, J., 2007. Non-intrusive characterization of the redox potential of landfill leachate plumes from self-potential data, *Journal of Contaminant Hydrology*, **92**, 274-292.

Aubert, M., and Yéené Atangana, Q., 1996. Self-potential method in hydrogeological exploration of volcanic areas, *Ground Water*, **34**, 1010-1016.

Avseth, P., Mukerji, T., Jørstad, A., Mavko, G., and Veggeland, T., 2001. Seismic reservoir mapping from 3-D AVO in a North Sea turbidite system, *Geophysics*, **66**, 1157-1176.

BAFU, 2010. Hydrologischer Atlas der Schweiz, *Bundeamt für Umwelt, Bern, Switzerland*.

Barrash, W., and Clemo, T., 2002. Hierarchical geostatistics and multifacies systems: Boise Hydrogeophysical Research Site, Boise, Idaho, *Water Resources Research*, **38**, 1196.

Barrenetxea, G., Ingelrest, F., Schaefer, G., and Vetterli, M., 2008. The hitchhiker's guide to successful wireless sensor network deployments, *Sensys'08: Proceedings of the 6th Acm Conference on Embedded Networked Sensor Systems*, 43-56.

Battin, T. J., and Sengschmitt, D., 1999. Linking sediment biofilms, hydrodynamics, and river bed clogging: Evidence from a large river, *Microbial Ecology*, **37**, 185-196.

Baumann, M., Jordan, P., Hoehn, E., and Geisser, H., 2009. Ein neues Grundwassermodell für das Thurtal, *Mitteilungen der Thurgauischen Naturforschenden Gesellschaft*, **63**.

Bedrosian, P. A., Maercklin, N., Weckmann, U., Bartov, Y., Ryberg, T., and Ritter, O., 2007. Lithology-derived structure classification from the joint interpretation of magnetotelluric and seismic models, *Geophysical Journal International*, **170**, 737-748.

Bélanger, C., Giroux, B., Gloaguen, E., and Lefebvre, R., 2010. GPR, ERT and CPT data integration for high resolution aquifer modeling, *13th International Conference on GPR*, 1-6.

Belghoul, A., 2007. *Caractérisation petrophysique et hydrodynamique du socle cristallin*: PhD thesis, University of Montpellier.

Belina, F. A., Ernst, J. R., and Holliger, K., 2009. Inversion of crosshole seismic data in heterogeneous environments: Comparison of waveform and ray-based approaches, *Journal of Applied Geophysics*, **68**, 85-94.

Bencala, K. E., 1984. Interactions of solutes and streambed sediment 2. A dynamic analysis of coupled hydrologic and chemical processes that determine solute transport, *Water Resources Research*, **20**, 1804-1814.

Beres, M., Green, A., Huggenberger, P., and Horstmeyer, H., 1995. Mapping the architecture of glaciofluvial sediments with 3-dimensional georadar, *Geology*, **23**, 1087-1090.

Beres, M., Huggenberger, P., Green, A. G., and Horstmeyer, H., 1999. Using two- and three-dimensional georadar methods to characterize glaciofluvial architecture, *Sedimentary Geology*, **129**, 1-24.

Bernhardt, E. S., Palmer, M. A., Allan, J. D., Alexander, G., Barnas, K., et al., 2005. Ecology - Synthesizing US river restoration efforts, *Science*, **308**, 636-637.

Beutel, J., Dyer, M., Lim, R., Plessl, C., Wohrle, M., et al., 2007. Automated wireless sensor network testing, *INSS 07: Proceedings of the Fourth International Conference on Networked Sensing Systems*, 303-303.

Beven, K., and Binley, A., 1992. The future of distributed models - model calibration and uncertainty prediction, *Hydrological Processes*, **6**, 279-298.

Bing, Z., and Greenhalgh, S. A., 1998a. A damping method for the computation of the 2.5-D Green's function for arbitrary acoustic media, *Geophysical Journal International*, **133**, 111-120.

Bing, Z., and Greenhalgh, S. A., 1998b. Crosshole acoustic velocity imaging with full-waveform spectral data: 2.5-D numerical simulations, *Exploration Geophysics*, **29**, 680-684.

Bing, Z., and Greenhalgh, S. A., 2000. Cross-hole resistivity tomography using different electrode configurations, *Geophysical Prospecting*, **48**, 887-912.

Binley, A., Winship, P., Middleton, R., Pokar, M., and West, J., 2001. High-resolution characterization of vadose zone dynamics using cross-borehole radar, *Water Resources Research*, **37**, 2639-2652.

Binley, A., Winship, P., West, L. J., Pokar, M., and Middleton, R., 2002a. Seasonal variation of moisture content in unsaturated sandstone inferred from borehole radar and resistivity profiles, *Journal of Hydrology*, **267**, 160-172.

Binley, A., Cassiani, G., Middleton, R., and Winship, P., 2002b. Vadose zone flow model parameterisation using cross-borehole radar and resistivity imaging, *Journal of Hydrology*, **267**, 147-159.

Binley, A., Cassiani, G., and Deiana, R., 2010. Hydrogeophysics: Opportunities and challenges, *Bollettino di Geofisica Teorica ed Applicata*, **51**, 267-284.

Birchak, J. R., Gardner, C. G., Hipp, J. E., and Victor, J. M., 1974. High dielectric constant microwave probes for sensing soil moisture, *Proceedings of the IEEE*, **62**, 93-98.

Bleistein, N., 1986. 2-1/2 dimensional inplane wave-propagation, *Geophysical Prospecting*, **34**, 686-703.

Blome, M., Maurer, H. R., and Schmidt, K., 2009. Advances in three-dimensional geoelectric forward solver techniques, *Geophysical Journal International*, **176**, 740-752.

Blome, M., Maurer, H., and Greenhalgh, S., 2011. Geoelectric experimental design - Efficient acquisition and exploitation of complete pole-bipole data sets, *Geophysics*, **76**, F15-F26.

Boggs, J. M., and Adams, E. E., 1992. Field study of dispersion in a heterogeneous aquifer: 4. Investigation of adsorption and sampling bias, *Water Resources Research*, **28**, 3325-3336.

Boggs, J. M., Young, S. C., Beard, L. M., Gelhar, L. W., Rehfeldt, K. R., and Adams, E. E., 1992. Field-study of dispersion in a heterogeneous aquifer: 1. Overview and site description, *Water Resources Research*, **28**, 3281-3291.

Bohlen, T., 2002. Parallel 3-D viscoelastic finite difference seismic modelling, *Computers & Geosciences*, **28**, 887-899.

Bolève, A., Revil, A., Janod, F., Mattiuzzo, J. L., and Fry, J. J., 2009. Preferential fluid flow pathways in embankment dams imaged by self-potential tomography, *Near Surface Geophysics*, **7**, 447-462.

Bosma, T. N. P., Ballemans, E. M. W., Hoekstra, N. K., teWelscher, R. A. G., Smeenk, J. G. M. M., et al., 1996. Biotransformation of organics in soil columns and an infiltration area, *Ground Water*, **34**, 49-56.

Bouman, C. A., 1997. Cluster: An unsupervised algorithm for modeling Gaussian mixtures, http://www.ece.purdue.edu/~bouman.

Bourg, A. C. M., and Bertin, C., 1993. Biogeochemical processes during the infiltration of river water into an alluvial aquifer, *Environmental Science & Technology*, **27**, 661-666.

Bouwer, H., and Rice, R. C., 1976. Slug test for determining hydraulic conductivity of unconfined aquifers with completely or partially penetrating wells, *Water Resources Research*, **12**, 423-428.

Bowling, J. C., Rodriguez, A. B., Harry, D. L., and Zheng, C., 2005. Delineating alluvial aquifer heterogeneity using resistivity and GPR data, *Ground Water*, **43**, 890-903.

Bowling, J. C., Harry, D. L., Rodriguez, A. B., and Zheng, C., 2007. Integrated geophysical and geological investigation of a heterogeneous fluvial aquifer in Columbus Mississippi, *Journal of Applied Geophysics*, **62**, 58-73.

Bradford, J. H., Clement, W. P., and Barrash, W., 2009. Estimating porosity with ground-penetrating radar reflection tomography: A controlled 3-D experiment at the Boise Hydrogeophysical Research Site, *Water Resources Research*, **45**, W00D26.

Brookes, A., 1988. *Channelized rivers: Prospectives for environmental management*, John Wiley and Sons, Chichester, UK.

Brovelli, A., and Cassiani, G., 2010. A combination of the Hashin-Shtrikman bounds aimed at modelling electrical conductivity and permittivity of variably saturated porous media, *Geophysical Journal International*, **180**, 225-237.

Brunke, M., and Gonser, T., 1997. The ecological significance of exchange processes between rivers and groundwater, *Freshwater Biology*, **37**, 1-33.

Butler, A. P., Mathias, S. A., Gallagher, A. J., Peach, D. W., and Williams, A. T., 2009. Analysis of flow processes in fractured chalk under pumped and ambient conditions (UK), *Hydrogeology Journal*, **17**, 1849-1858.

Butler, J. J., 1998. *The design, performance and analysis of slug tests*, Lewis, Boca Raton.

Butler, J. J., Garnett, E. J., and Healey, J. M., 2003. Analysis of slug tests in formations of high hydraulic conductivity, *Ground Water*, **41**, 620-630.

BUWAL, 2004. Wegleitung Grundwasserschutz, *Bundesamt für Umwelt, Wald und Landschaft, Bern, Switzerland*.

Carcione, J. M., Ursin, B., and Nordskag, J. I., 2007. Cross-property relations between electrical conductivity and the seismic velocity of rocks, *Geophysics*, **72**, E193-E204.

Cardenas, M. B., Wilson, J. L., and Zlotnik, V. A., 2004. Impact of heterogeneity, bed forms, and stream curvature on subchannel hyporheic exchange, *Water Resources Research*, **40**, W08307.

Cardenas, M. B., and Markowski, M. S., 2011. Geoelectrical imaging of hyporheic exchange and mixing of river water and groundwater in a large regulated river, *Environmental Science & Technology*, **45**, 1407-1411.

Carsel, R. F., and Parrish, R. S., 1988. Developing joint probability-distributions of soil-water retention characteristics, *Water Resources Research*, **24**, 755-769.

Caruthers, R. M., and Smith, I. F., 1992. The use of ground electrical survey methods for siting water-supply boreholes in shallow crystalline basement terrains, in *Hydrogeology of Crystalline Basement Aquifers in Africa*, edited by E. P. Wright and W. G. Burgess, pp. 203-220, Geological Society Special Publication.

Cassiani, G., Bruno, V., Villa, A., Fusi, N., and Binley, A. M., 2006. A saline trace test monitored via time-lapse surface electrical resistivity tomography, *Journal of Applied Geophysics*, **59**, 244-259.

Chambers, J. E., Wilkinson, P. B., Weller, A. L., Meldrum, P. I., Gilvy, R. D., and Caunt, S., 2007. Mineshaft imaging using surface and crosshole 3D electrical resistivity tomography: A case history from the East Pennine Coalfield, UK, *Journal of Applied Geophysics*, **62**, 324-337.

Chen, J. S., Hubbard, S., Rubin, Y., Murray, C., Roden, E., and Majer, E., 2004. Geochemical characterization using geophysical data and Markov Chain Monte Carlo methods: A case

study at the South Oyster bacterial transport site in Virginia, *Water Resources Research*, **40**, W12412.

Cirpka, O. A., Fienen, M. N., Hofer, M., Hoehn, E., Tessarini, A., et al., 2007. Analyzing bank filtration by deconvoluting time series of electric conductivity, *Ground Water*, **45**, 318-328.

Claerbout, J. F., and Muir, F., 1973. Robust modeling with erratic data, *Geophysics*, **38**, 826-844.

Constantz, J., Cox, M. H., and Su, G. W., 2003. Comparison of heat and bromide as ground water tracers near streams, *Ground Water*, **41**, 647-656.

Constantz, J., 2008. Heat as a tracer to determine streambed water exchanges, *Water Resources Research*, **44**, W00D10.

Coscia, I., Marescot, L., Maurer, H., Greenhalgh, S., and Linde, N., 2008. Experimental design for crosshole electrical resistivity tomography data sets, *14th Annual European Meeting of Environmental and Engineering Geophysics, EAGE.*

Coscia, I., Greenhalgh, S., Linde, N., Green, A., Günther, T., et al., 2010. A multi-borehole 3-D ERT monitoring system for aquifer characterization using river flood events as a natural tracer, *16th Annual European Meeting of Environmental and Engineering Geophysics, EAGE.*

Coscia, I., Greenhalgh, S. A., Linde, N., Doetsch, J., Marescot, L., et al., 2011a. 3D crosshole ERT for aquifer characterization and monitoring of infiltrating river water, *Geophysics*, **76**, G49-G59.

Coscia, I., Linde, N., Greenhalgh, S., Günther, T., and Green, A., 2011b. A deconvolution approach to correct time-lapse 3D ERT data and improve imaging of natural aquifer dynamics, *Water Resources Research*, under review.

Crook, N., Binley, A., Knight, R., Robinson, D. A., Zarnetske, J., and Haggerty, R., 2008. Electrical resistivity imaging of the architecture of substream sediments, *Water Resources Research*, **44**, W00D13.

Daily, W., and Owen, E., 1991. Cross-borehole resistivity tomography, *Geophysics*, **56**, 1228-1235.

Daily, W., Ramirez, A., Labrecque, D., and Nitao, J., 1992. Electrical resistivity tomography of vadose water movement, *Water Resources Research*, **28**, 1429-1442.

Daily, W., and Ramirez, A., 1995. Electrical-resistance tomography during in-situ trichloroethylene remediation at the savanna river site, *Journal of Applied Geophysics*, **33**, 239-249.

Daily, W., Ramirez, A., Binley, A., and LaBrecque, D., 2005. Electrical resistance tomography — theory and practice, in *Near surface geophysics*, edited by D. K. Butler, pp. 525-550, SEG.

Daniels, J. J., Allred, B., Binley, A., Labrecque, D., and Alumbaugh, D., 2005. Hydrogeophysical case studies in the vadose zone, in *Hydrogeophysics*, edited by Y. Rubin and S. S. Hubbard, pp. 413-440, Springer.

Darling, T., 2005. *Well logging and formation evaluation*, Elsevier.

Darnet, M., and Marquis, G., 2004. Modelling streaming potential (SP) signals induced by water movement in the vadose zone, *Journal of Hydrology*, **285**, 114-124.

Day-Lewis, F. D., Lane, J. W., Jr., Harris, J. M., and Gorelick, S. M., 2003. Time-lapse imaging of saline-tracer transport in fractured rock using difference-attenuation radar tomography, *Water Resources Research*, **39**, 1290.

Day-Lewis, F. D., and Lane, J. W., 2004. Assessing the resolution-dependent utility of tomograms for geostatistics, *Geophysical Research Letters*, **31**, L07503.

Day-Lewis, F. D., Singha, K., and Binley, A. M., 2005. Applying petrophysical models to radar travel time and electrical resistivity tomograms: Resolution-dependent limitations, *Journal of Geophysical Research-Solid Earth*, **110**, B08206.

Day-Lewis, F. D., Lane, J. W., and Gorelick, S. M., 2006. Combined interpretation of radar, hydraulic, and tracer data from a fractured-rock aquifer near Mirror Lake, New Hampshire, USA, *Hydrogeology Journal*, **14**, 1-14.

Day-Lewis, F. D., Chen, Y., and Singha, K., 2007. Moment inference from tomograms, *Geophysical Research Letters*, **34**, L22404.

de Franco, R., Biella, G., Tosi, L., Teatini, P., Lozej, A., et al., 2009. Monitoring the saltwater intrusion by time lapse electrical resistivity tomography: The Chioggia test site (Venice Lagoon, Italy), *Journal of Applied Geophysics*, **69**, 117-130.

Deiana, R., Cassiani, G., Kemna, A., Villa, A., Bruno, V., and Bagliani, A., 2007. An experiment of non-invasive characterization of the vadose zone via water injection and cross-hole time-lapse geophysical monitoring, *Near Surface Geophysics*, **5**, 183-194.

Dempster, A. P., Laird, N. M., and Rubin, D. B., 1977. Maximum likelihood from incomplete data via the EM algorithm, *Journal of the Royal Statistical Society, Series B (Methodological)*, **39**, 1-38.

Deutsch, C. V., and Journel, A. G., 1998. *GSLIB: Geostatistical software library and user's guide*, 2. edition ed., Oxford Univ. Press, New York, 2. edition.

Diem, S., Vogt, T., and Hoehn, E., 2010. Räumliche Charakterisierung der hydraulischen Leitfähigkeit in alluvialen Schotter-Grundwasserleitern: Ein Methodenvergleich, *Grundwasser*, **15**, 241-251.

Dietrich, C. R., and Newsam, G. N., 1997. Fast and exact simulation of stationary Gaussian processes through circulant embedding of the covariance matrix, *Siam Journal on Scientific Computing*, **18**, 1088-1107.

Dogan, M., Van Dam, R. L., Bohling, G. C., Butler, J. J., Jr., and Hyndman, D. W., 2011. Hydrostratigraphic analysis of the MADE site with full-resolution GPR and direct-push hydraulic profiling, *Geophysical Research Letters*, **38**, L06405.

Dorn, C., Linde, N., Le Borgne, T., Bour, O., and Baron, L., 2011. Single-hole GPR reflection imaging of solute transport in a granitic aquifer, *Geophysical Research Letters*, **38**, L08401.

Doussan, C., Jouniaux, L., and Thony, J. L., 2002. Variations of self-potential and unsaturated water flow with time in sandy loam and clay loam soils, *Journal of Hydrology*, **267**, 173-185.

EC, 2000. Directive 2000/60/EC of the European Parliament and of the council establishing a framework for community action in the field of water policy, *Official Journal of the European Community*, **L327**, 1-72.

Eckert, P., Lamberts, R., and Wagner, C., 2008. The impact of climate change on drinking water supply by riverbank filtration, *Water Science Technology*, **8**, 319-324.

Edmaier, K., Burlando, P., and Perona, P., 2011. Mechanisms of vegetation uprooting by flow in alluvial non-cohesive sediment, *Hydrology and Earth Systems Science Discussion*, **8**, 1365-1398.

Eisenberg, D., and Kauzmann, W., 1969. *The structure and properties of water*, Oxford University Press.

Ellis, R. G., and Oldenburg, D. W., 1994. Applied geophysical inversion, *Geophysical Journal International*, **116**, 5-11.

Eppstein, M. J., and Dougherty, D. E., 1998. Optimal 3-D traveltime tomography, *Geophysics*, **63**, 1053-1061.

Ernst, J. R., Maurer, H., Green, A. G., and Holliger, K., 2007a. Full-waveform inversion of crosshole radar data based on 2-D finite-difference time-domain solutions of Maxwell's equations, *Ieee Transactions on Geoscience and Remote Sensing*, **45**, 2807-2828.

Ernst, J. R., Green, A. G., Maurer, H., and Holliger, K., 2007b. Application of a new 2D time-domain full-waveform inversion scheme to crosshole radar data, *Geophysics*, **72**, J53-J64.

Ernst, J. R., 2007. *2-D finite-difference time-domain full-waveform inversion of crosshole georadar data*: PhD thesis, ETH Zurich.

Farquharson, C. G., 2008. Constructing piecewise-constant models in multidimensional minimum-structure inversions, *Geophysics*, **73**, K1-K9.

Favetto, A., Pomposiello, C., Booker, J., and Rossello, E. A., 2007. Magnetotelluric inversion constrained by seismic data in the Tucuman basin (Andean foothills, 27 degrees S, NW argentina), *Journal of Geophysical Research - Solid Earth*, **112**, B09104.

Fine, R. A., and Millero, F. J., 1973. Compressibility of water as a function of temperature and pressure, *Journal of Chemical Physics*, **59**, 5529-5536.

Fleckenstein, J. H., Niswonger, R. G., and Fogg, G. E., 2006. River-aquifer interactions, geologic heterogeneity, and low-flow management, *Ground Water*, **44**, 837-852.

Fournier, C., 1989. Spontaneous potentials and resistivity surveys applied to hydrogeology in a volcanic area - case-history of the Chaine-Des-Puys (Puy-De-Dome, France), *Geophysical Prospecting*, **37**, 647-668.

Fregoso, E., and Gallardo, L. A., 2009. Cross-gradients joint 3D inversion with applications to gravity and magnetic data, *Geophysics*, **74**, L31-L42.

French, H., and Binley, A., 2004. Snowmelt infiltration: Monitoring temporal and spatial variability using time-lapse electrical resistivity, *Journal of Hydrology*, **297**, 174-186.

Friedel, S., 2003. Resolution, stability and efficiency of resistivity tomography estimated from a generalized inverse approach, *Geophysical Journal International*, **153**, 305-316.

Friedel, S., Byrdina, S., Jacobs, F., and Zimmer, M., 2004. Self-potential and ground temperature at Merapi volcano prior to its crisis in the rainy season of 2000-2001, *Journal of Volcanology and Geothermal Research*, **134**, 149-168.

Füchtenbauer, H., 1988. *Sedimente und Sedimentgesteine: Sandsteine*, 4 ed., Schweizerbart, Stuttgart.

Gallardo, L. A., and Meju, M. A., 2003. Characterization of heterogeneous near-surface materials by joint 2D inversion of dc resistivity and seismic data, *Geophysical Research Letters*, **30**, 1658.

Gallardo, L. A., and Meju, M. A., 2004. Joint two-dimensional DC resistivity and seismic travel time inversion with cross-gradients constraints, *Journal of Geophysical Research - Solid Earth*, **109**, B03311.

Gallardo, L. A., Meju, M. A., and Pérez-Flores, M. A., 2005. A quadratic programming approach for joint image reconstruction: Mathematical and geophysical examples, *Inverse Problems*, **21**, 435-452.

Gallardo, L. A., 2007. Multiple cross-gradient joint inversion for geospectral imaging, *Geophysical Research Letters*, **34**, L19301.

Gallardo, L. A., and Meju, M. A., 2007. Joint two-dimensional cross-gradient imaging of magnetotelluric and seismic traveltime data for structural and lithological classification, *Geophysical Journal International*, **169**, 1261-1272.

Gallardo, L. A., and Meju, M. A., 2011. Structure-Coupled Multiphysics Imaging in Geophysical Sciences, *Reviews of Geophysics*, **49**, RG1003.

Garambois, S., Senechal, P., and Perroud, H., 2002. On the use of combined geophysical methods to assess water content and water conductivity of near-surface formations, *Journal of Hydrology*, **259**, 32-48.

Gasperikova, E., Zhang, Y., and Hubbard, S., 2008. Using self potential and multiphase flow modeling to optimize groundwater pumping*, EOS Transactions AGU, 89(53).*

Giannopoulos, A., 2005. Modelling ground penetrating radar by GprMax, *Construction and Building Materials*, **19**, 755-762.

Gibert, D., and Pessel, M., 2001. Identification of sources of potential fields with the continuous wavelet transform: Application to self-potential profiles, *Geophysical Research Letters*, **28**, 1863-1866.

Golub, G. H., and van Loan, C. F., 1996. *Matrix computations*, Johns Hopkins University Press.

Gooseff, M. N., Anderson, J. K., Wondzell, S. M., LaNier, J., and Haggerty, R., 2005. A modelling study of hyporheic exchange pattern and the sequence, size, and spacing of stream bedforms in mountain stream networks, Oregon, USA, *Hydrological Processes*, **19**, 2915-2929.

Grasmueck, M., 1996. 3-D ground-penetrating radar applied to fracture imaging in gneiss, *Geophysics*, **61**, 1050-1064.

Grinsted, A., Moore, J. C., and Jevrejeva, S., 2004. Application of the cross wavelet transform and wavelet coherence to geophysical time series, *Nonlinear Processes in Geophysics*, **11**, 561-566.

GschG, 1991. Gewaesserschutzgesetz,, *Bundesgesetz über den Schutz der Gewässer, Schweiz*, **814.20**, 30.

GSchV, 1998. Gewaesserschutzverordnung, *Bundesgesetz über den Schutz der Gewässer, Schweiz*, **814.201**, 60.

Günther, T., 2004. *Inversion methods and resolution analysis for the 2D/3D reconstruction of resistivity structures from DC measurements*, Ph.D. thesis thesis: TU Bergakademie Freiberg.

Günther, T., and Rücker, C., 2006. A general approach for introducing information into inversion and examples from dc resistivity inversion, in *14th Annual European Meeting of Environmental and Engineering Geophysics*, edited, p. P039, EAGE.

Günther, T., Rücker, C., and Spitzer, K., 2006. Three-dimensional modelling and inversion of dc resistivity data incorporating topography - II. Inversion, *Geophysical Journal International*, **166**, 506-517.

Günther, T., and Rücker, C., 2009. Advanced inversion strategies using a new geophysical inversion and modelling library, *15th Annual European Meeting of Environmental and Engineering Geophysics, EAGE.*

Haber, E., and Oldenburg, D., 1997. Joint inversion: A structural approach, *Inverse Problems*, **13**, 63-77.

Harbaugh, A. W., 2005. MODFLOW-2005, The U.S. Geological Survey modular ground-water model—the ground-water flow process, in *Book 6. Modeling techniques*, Ch. 16.

Harvey, J. W., and Bencala, K. E., 1993. The effect of streambed topography on surface-subsurface water exchange in mountain catchments, *Water Resources Research*, **29**, 89-98.

Hashin, Z., and Shtrikman, S., 1962. A variational approach to theory of effective magnetic permeability of multiphase materials, *Journal of Applied Physics*, **33**, 3125-&.

Hashin, Z., and Shtrikman, S., 1963. A variational approach to the theory of the elastic behaviour of multiphase materials, *Journal of the Mechanics and Physics of Solids*, **11**, 127-140.

Hatch, C. E., Fisher, A. T., Revenaugh, J. S., Constantz, J., and Ruehl, C., 2006. Quantifying surface water-groundwater interactions using time series analysis of streambed thermal records: Method development, *Water Resources Research*, **42**, W10410.

Hauck, C., 2002. Frozen ground monitoring using DC resistivity tomography, *Geophysical Research Letters*, **29**, 2016.

Hayley, K., Bentley, L. R., and Gharibi, M., 2009. Time-lapse electrical resistivity monitoring of salt-affected soil and groundwater, *Water Resources Research*, **45**.

Heinz, J., Kleineidam, S., Teutsch, G., and Aigner, T., 2003. Heterogeneity patterns of quaternary glaciofluvial gravel bodies (SW-Germany): Application to hydrogeology, *Sedimentary Geology*, **158**, 1-23.

Henderson, R. D., Day-Lewis, F. D., and Harvey, C. F., 2009. Investigation of aquifer-estuary interaction using wavelet analysis of fiber-optic temperature data, *Geophysical Research Letters*, **36**, L06403.

Hiscock, K. M., and Grischek, T., 2002. Attenuation of groundwater pollution by bank filtration, *Journal of Hydrology*, **266**, 139-144.

Hoehn, E., and Cirpka, O. A., 2006. Assessing residence times of hyporheic ground water in two alluvial flood plains of the Southern Alps using water temperature and tracers, *Hydrology and Earth System Sciences*, **10**, 553-563.

Hoehn, E., and Scholtis, A., 2011. Exchange between a river and groundwater, assessed with hydrochemical data, *Hydrology and Earth System Sciences*, **15**, 983-988.

Hollender, F., Tillard, S., and Corin, L., 1999. Multifold borehole radar acquisition and processing, *Geophysical Prospecting*, **47**, 1077-1090.

Holliger, K., Musil, M., and Maurer, H. R., 2001. Ray-based amplitude tomography for crosshole georadar data: A numerical assessment, *Journal of Applied Geophysics*, **47**, 285-298.

Hu, W. Y., Abubakar, A., and Habashy, T. M., 2009. Joint electromagnetic and seismic inversion using structural constraints, *Geophysics*, **74**, R99-R109.

Hubbard, S., and Linde, N., 2011. Hydrogeophysics, in *Treatise on water*, edited by P. Wilderer, Ch. 43, Elsevier.

Hubbard, S. S., Rubin, Y., and Majer, E., 1999. Spatial correlation structure estimation using geophysical and hydrogeological data, *Water Resources Research*, **35**, 1809-1825.

Hubbard, S. S., Chen, J. S., Peterson, J., Majer, E. L., Williams, K. H., et al., 2001. Hydrogeological characterization of the South Oyster Bacterial Transport Site using geophysical data, *Water Resources Research*, **37**, 2431-2456.

Huggenberger, P., 1993. Radar facies: Recognition of facies patterns and heterogeneities within Pleistocene Rhine gravels, NE Switzerland, *Geological Society, London, Special Publications*, **75**, 163-176.

Huggenberger, P., Hoehn, E., Beschta, R., and Woessner, W., 1998. Abiotic aspects of channels and floodplains in riparian ecology, *Freshwater Biology*, **40**, 407-425.

Hyndman, D. W., and Gorelick, S. M., 1996. Estimating lithologic and transport properties in three dimensions using seismic and tracer data: The Kesterson aquifer, *Water Resources Research*, **32**, 2659-2670.

Hyndman, D. W., and Harris, J. M., 1996. Traveltime inversion for the geometry of aquifer lithologies, *Geophysics*, **61**, 1728-1737.

Jackson, M. D., 2010. Multiphase electrokinetic coupling: Insights into the impact of fluid and charge distribution at the pore scale from a bundle of capillary tubes model, *Journal of Geophysical Research-Solid Earth*, **115**, B07206.

Jacobs, L. A., Vongunten, H. R., Keil, R., and Kuslys, M., 1988. Geochemical changes along a river-groundwater infiltration flow path - Glattfelden, Switzerland, *Geochimica Et Cosmochimica Acta*, **52**, 2693-2706.

Jakubowicz, H., 1990. A simple efficient method of dip-moveout correction, *Geophysical Prospecting*, **38**, 221-245.

Jardani, A., Revil, A., Boleve, A., Crespy, A., Dupont, J. P., et al., 2007. Tomography of the Darcy velocity from self-potential measurements, *Geophysical Research Letters*, **34**, L24403.

Jayawickreme, D. H., Van Dam, R. L., and Hyndman, D. W., 2008. Subsurface imaging of vegetation, climate, and root-zone moisture interactions, *Geophysical Research Letters*, **35**, L18404.

Jegen, M. D., Hobbs, R. W., Tarits, P., and Chave, A., 2009. Joint inversion of marine magnetotelluric and gravity data incorporating seismic constraints: Preliminary results of sub-basalt imaging off the Faroe Shelf, *Earth and Planetary Science Letters*, **282**, 47-55.

Jougnot, D., Ghorbani, A., Revil, A., Leroy, P., and Cosenza, P., 2010. Spectral induced polarization of partially saturated clay-rocks: A mechanistic approach, *Geophysical Journal International*, **180**, 210-224.

Jung, H. K., Min, D. J., Lee, H. S., Oh, S., and Chung, H., 2009. Negative apparent resistivity in dipole-dipole electrical surveys, *Exploration Geophysics*, **40**, 33-40.

Kalbus, E., Reinstorf, F., and Schirmer, M., 2006. Measuring methods for groundwater - surface water interactions: A review, *Hydrology and Earth System Sciences*, **10**, 873-887.

Kalbus, E., Schmidt, C., Molson, J. W., Reinstorf, F., and Schirmer, M., 2009. Influence of aquifer and streambed heterogeneity on the distribution of groundwater discharge, *Hydrology and Earth System Sciences*, **13**, 69-77.

Keery, J., Binley, A., Crook, N., and Smith, J. W. N., 2007. Temporal and spatial variability of groundwater-surface water fluxes: Development and application of an analytical method using temperature time series, *Journal of Hydrology*, **336**, 1-16.

Keller, G. V., and Frischknecht, F., 1966. *Electrical methods in geophysical prospecting*, Pergamon.

Kemna, A., Kulessa, B., and Vereecken, H., 2002. Imaging and characterisation of subsurface solute transport using electrical resistivity tomography (ERT) and equivalent transport models, *Journal of Hydrology*, **267**, 125-146.

Khalil, A. A., Stewart, R. R., and Henley, D. C., 1993. Full-wave-form processing and interpretation of kilohertz cross-well seismic data, *Geophysics*, **58**, 1248-1256.

Kipfer, R., Aeschbach-Hertig, W., Peeters, F., and Stute, M., 2002. Noble gases in lakes and ground waters, *Noble Gases in Geochemistry and Cosmochemistry*, **47**, 615-700.

Klotzsche, A., van der Kruk, J., Meles, G. A., Doetsch, J., Maurer, H., and Linde, N., 2010. Full-waveform inversion of cross-hole ground-penetrating radar data to characterize a gravel aquifer close to the Thur River, Switzerland, *Near Surface Geophysics*, **8**, 635-649.

Knight, R. J., and Nur, A., 1987. The dielectric-constant of sandstones, 60 Khz to 4 Mhz, *Geophysics*, **52**, 644-654.

Koch, K., Wenninger, J., Uhlenbrook, S., and Bonell, M., 2009. Joint interpretation of hydrological and geophysical data: Electrical resistivity tomography results from a process hydrological research site in the Black Forest Mountains, Germany, *Hydrological Processes*, **23**, 1501-1513.

Kondolf, G. M., 1998. Lessons learned from river restoration projects in California, *Aquatic Conservation-Marine and Freshwater Ecosystems*, **8**, 39-52.

Kosinski, W. K., and Kelly, W. E., 1981. Geoelectric soundings for predicting aquifer properties, *Ground Water*, **19**, 163-171.

Kowalsky, M. B., Finsterle, S., Peterson, J., Hubbard, S., Rubin, Y., et al., 2005. Estimation of field-scale soil hydraulic and dielectric parameters through joint inversion of GPR and hydrological data, *Water Resources Research*, **41**, W11425.

Krautblatter, M., Verleysdonk, S., Flores-Orozco, A., and Kemna, A., 2010. Temperature-calibrated imaging of seasonal changes in permafrost rock walls by quantitative electrical resistivity

tomography (Zugspitze, German/Austrian Alps), *Journal of Geophysical Research-Earth Surface*, **115**, F02003.

Kruse, S., Grasmueck, M., Weiss, M., and Viggiano, D., 2006. Sinkhole structure imaging in covered Karst terrain, *Geophysical Research Letters*, **33**, L16405.

Kumar, P., and Foufoula-Georgiou, E., 1997. Wavelet analysis for geophysical applications, *Reviews of Geophysics*, **35**, 385-412.

Kuras, O., Pritchard, J. D., Meldrum, P. I., Chambers, J. E., Wilkinson, P. B., et al., 2009. Monitoring hydraulic processes with automated time-lapse electrical resistivity tomography (ALERT), *Comptes Rendus Geoscience*, **341**, 868-885.

Kuroda, S., Takeuchi, M., and Kim, H. J., 2007. Full-waveform inversion algorithm for interpreting crosshole radar data: A theoretical approach, *Geosciences Journal*, **11**, 211-217.

LaBrecque, D. J., Ramirez, A. L., Daily, W. D., Binley, A. M., and Schima, S. A., 1996a. ERT monitoring on environmental remediation processes, *Measurement Science & Technology*, **7**, 375-383.

LaBrecque, D. J., Miletto, M., Daily, W., Ramirez, A., and Owen, E., 1996b. The effects of noise on Occam's inversion of resistivity tomography data, *Geophysics*, **61**, 538-548.

LaBrecque, D. J., and Yang, X., 2001. Difference inversion of ERT data: A fast inversion method for 3-D in situ monitoring, *Journal of Environmental and Engineering Geophysics*, **6**, 83-89.

Lacey, G., 1930. Stable channel in alluvium, *Proceedings of the Institution of Civil Engineers*, **229**, 259-292.

Lane, J. W., Day-Lewis, F. D., and Casey, C. C., 2006. Geophysical monitoring of a field-scale biostimulation pilot project, *Ground Water*, **44**, 430-443.

Langevin, C. D., Thorne, D. T., Jr., Dausman, A. M., Sukip, M. C., and Guo, W., 2008. SEAWAT version 4: A computer program for simulation of multi-species solute and heat transport, in *USGS Techniques and Methods Book 6*, Ch. A22.

Langevin, C. D., 2009. SEAWAT: A computer program for simulation of variable-density groundwater flow and multi-species solute and heat transport, *U.S. Geological Survey*, Fact Sheet 2009-3047.

Lanz, E., Boerner, D. E., Maurer, H., and Green, A., 1998. Landfill delineation and characterization using electrical, electromagnetic and magnetic methods, *Journal of Environmental and Engineering Geophysics*, **3**, 185-196.

Lazaratos, S. K., Harris, J. M., Rector, J. W., and Vanschaack, M., 1995. High-resolution crosswell imaging of a west texas carbonate reservoir 4. Reflection imaging, *Geophysics*, **60**, 702-711.

Le Borgne, T., Bour, O., Paillet, F. L., and Caudal, J. P., 2006. Assessment of preferential flow path connectivity, and hydraulic properties at single-borehole and cross-borehole scales in a fractured aquifer, *Journal of Hydrology*, **328**, 347-359.

Le Borgne, T., Bour, O., Riley, M. S., Gouze, P., Pezard, P. A., et al., 2007. Comparison of alternative methodologies for identifying and characterizing preferential flow paths in heterogeneous aquifers, *Journal of Hydrology*, **345**, 134-148.

Leonard, B. P., 1991. The ULTIMATE conservative difference scheme applied to unsteady one-dimensional advection, *Computer Methods in Applied Mechanics and Engineering*, **88**, 17-74.

Lesmes, D. P., and Friedman, S. P., 2005. Relationships between the electrical and hydrogeological properties of rocks and soils, in *Hydrogeophysics*, edited by Y. Rubin and S. S. Hubbard, pp. 87-128, Springer.

Li, S. H., Unsworth, M. J., Booker, J. R., Wei, W. B., Tan, H. D., and Jones, A. G., 2003. Partial melt or aqueous fluid in the mid-crust of Southern Tibet? Constraints from INDEPTH magnetotelluric data, *Geophysical Journal International*, **153**, 289-304.

Linde, N., Binley, A., Tryggvason, A., Pedersen, L. B., and Revil, A., 2006a. Improved hydrogeophysical characterization using joint inversion of cross-hole electrical resistance and ground-penetrating radar traveltime data, *Water Resources Research*, **42**, W12404.

Linde, N., Finsterle, S., and Hubbard, S., 2006b. Inversion of tracer test data using tomographic constraints, *Water Resources Research*, **42**, W04410.

Linde, N., Jougnot, D., Revil, A., Matthäi, S. K., Arora, T., et al., 2007a. Streaming current generation in two-phase flow conditions, *Geophysical Research Letters*, **34**, L03306.

Linde, N., and Revil, A., 2007. Inverting self-potential data for redox potentials of contaminant plumes, *Geophysical Research Letters*, **34**, L14302.

Linde, N., Revil, A., Bolève, A., Dagès, C., Castermant, J., et al., 2007b. Estimation of the water table throughout a catchment using self-potential and piezometric data in a Bayesian framework, *Journal of Hydrology*, **334**, 88-98.

Linde, N., Tryggvason, A., Peterson, J. E., and Hubbard, S. S., 2008. Joint inversion of crosshole radar and seismic traveltimes acquired at the South Oyster Bacterial Transport Site, *Geophysics*, **73**, G29-G37.

Linde, N., and Doetsch, J. A., 2010. Joint inversion of crosshole GPR and seismic traveltime data, in *Advances in near-surface seismology and ground-penetrating radar*, edited by R. D. Miller, J. H. Bradford and K. Holliger, Ch. 1, pp. 1-18, Society of Exploration Geophysicists.

Linde, N., Doetsch, J., Jougnot, D., Genoni, O., Dürst, Y., et al., 2011. Self-potential investigations of a gravel bar in a restored river corridor, *Hydrology and Earth System Sciences*, **15**, 729-742.

Lines, L. R., Schultz, A. K., and Treitel, S., 1988. Cooperative inversion of geophysical data, *Geophysics*, **53**, 8-20.

Loke, M. H., and Barker, R. D., 1996. Practical techniques for 3D resistivity surveys and data inversion, *Geophysical Prospecting*, **44**, 499-523.

Long, J. C. S., Aydin, A., Brown, S. R., Einstein, H. H., Hestir, K., et al., 1996. *Rock fracture and fluid flow: Contemporary understanding and applications*, National Academy Press, Washington, DC.

Looms, M. C., Jensen, K. H., Binley, A., and Nielsen, L., 2008. Monitoring unsaturated flow and transport using cross-borehole geophysical methods, *Vadose Zone Journal*, **7**, 227.

Lowry, T., Allen, M. B., and Shive, P. N., 1989. Singularity removal: A refinement of resistivity modeling techniques, *Geophysics*, **54**, 766-774.

Lunt, I. A., Bridge, J. S., and Tye, R. S., 2004. A quantitative three-dimensional depositional model of gravelly braided rivers, *Sedimentology*, **51**, 1155-1155.

Maineult, A., Bernabe, Y., and Ackerer, P., 2004. Electrical response of flow, diffusion, and advection in a laboratory sand box, *Vadose Zone Journal*, **3**, 1180-1192.

Maineult, A., Bernabe, Y., and Ackerer, P., 2005. Detection of advected concentration and pH fronts from self-potential measurements, *Journal of Geophysical Research-Solid Earth*, **110**, B11205.

Maineult, A., Strobach, E., and Renner, J., 2008. Self-potential signals induced by periodic pumping tests, *Journal of Geophysical Research-Solid Earth*, **113**, B01203.

Mair, J. A., and Green, A. G., 1981. High-resolution seismic-reflection profiles reveal fracture-zones within a homogeneous granite batholith, *Nature*, **294**, 439-442.

Maraun, D., and Kurths, J., 2004. Cross wavelet analysis: Significance testing and pitfalls, *Nonlinear Processes in Geophysics*, **11**, 505-514.

Marescot, L., Rigobert, S., P. Lopes, S., Lagabrielle, R., and Chapellier, D., 2006. A general approach for DC apparent resistivity evaluation on arbitrarily shaped 3D structures, *Journal of Applied Geophysics*, **60**, 55-67.

Maurer, H., Holliger, K., and Boerner, D. E., 1998. Stochastic regularization: Smoothness or similarity?, *Geophysical Research Letters*, **25**, 2889-2892.

Maurer, H., and Musil, M., 2004. Effects and removal of systematic errors in crosshole georadar attenuation tomography, *Journal of Applied Geophysics*, **55**, 261-270.

Maurer, H., and Friedel, S., 2006. Outer-space sensitivities in geoelectrical tomography, *Geophysics*, **71**, G93-G96.

Maurer, H., Friedel, S., and Jaeggi, D., 2009. Characterization of a coastal aquifer using seismic and geoelectric borehole methods, *Near Surface Geophysics*, **7**, 353-366.

Mazac, O., Kelly, W. E., and Landa, I., 1987. Surface geoelectrics for groundwater pollution and protection studies, *Journal of Hydrology*, **93**, 277-294.

McClymont, A. F., Green, A. G., Streich, R., Horstmeyer, H., Tronicke, J., et al., 2008. Visualization of active faults using geometric attributes of 3D GPR data: An example from the Alpine Fault Zone, New Zealand, *Geophysics*, **73**, B11-B23.

McElwee, C. D., and Zenner, M. A., 1998. A nonlinear model for analysis of slug-test data, *Water Resources Research*, **34**, 55-66.

Meles, G. A., Van der Kruk, J., Greenhalgh, S. A., Ernst, J. R., Maurer, H., and Green, A. G., 2010. A new vector waveform inversion algorithm for simultaneous updating of conductivity and permittivity parameters from combination crosshole/borehole-to-surface GPR data, *Ieee Transactions on Geoscience and Remote Sensing*, **48**, 3391-3407.

Merkli, B., 1975. *Untersuchungen über Mechanismen und Kinetik der Elimination von Bakterien und Viren im Grundwasser*: ETH Zurich.

Miall, A. D., 1995. Description and interpretation of fluvial deposits - A critical perspective, *Sedimentology*, **42**, 379-384.

Michel, S., Salehi, A., Luo, L., Dawes, N., Aberer, K., et al., 2009. Environmental monitoring 2.0, *Icde: 2009 Ieee 25th International Conference on Data Engineering, Vols. 1-3*, 1507-1510.

Michot, D., Benderitter, Y., Dorigny, A., Nicoullaud, B., King, D., and Tabbagh, A., 2003. Spatial and temporal monitoring of soil water content with an irrigated corn crop cover using surface electrical resistivity tomography, *Water Resources Research*, **39**, 1138.

Miller, C. R., Routh, P. S., Brosten, T. R., and McNamara, J. P., 2008. Application of time-lapse ERT imaging to watershed characterization, *Geophysics*, **73**, G7-G17.

Minsley, B. J., 2007. *Modeling and inversion of self-potential data*: PhD thesis, Massachusetts Institute of Technology.

Minsley, B. J., Sogade, J., and Morgan, F. D., 2007. Three-dimensional source inversion of self-potential data, *Journal of Geophysical Research*, **112**.

Mitchell, T. M., 1997. *Machine learning*, McGraw-Hill, New York.

Monego, M., Cassiani, G., Deiana, R., Putti, M., Passadore, G., and Altissimo, L., 2010. A tracer test in a shallow heterogeneous aquifer monitored via time-lapse surface electrical resistivity tomography, *Geophysics*, **75**, WA61-WA73.

Monteiro Santos, F. A., Sultan, S. A., Represas, P., and El Sorady, A. L., 2006. Joint inversion of gravity and geoelectrical data for groundwater and structural investigation: Application to the northwestern part of Sinai, Egypt, *Geophysical Journal International*, **165**, 705-718.

Mora, P., 1987. Nonlinear two-dimensional elastic inversion of multioffset seismic data, *Geophysics*, **52**, 1211-1228.

Müller, K., Vanderborght, J., Englert, A., Kemna, A., Huisman, J. A., et al., 2010. Imaging and characterization of solute transport during two tracer tests in a shallow aquifer using electrical resistivity tomography and multilevel groundwater samplers, *Water Resources Research*, **46**, W03502.

Musil, M., Maurer, H. R., and Green, A. G., 2003. Discrete tomography and joint inversion for loosely connected or unconnected physical properties: Application to crosshole seismic and georadar data sets, *Geophysical Journal International*, **153**, 389-402.

Nadeau, D. F., Brutsaert, W., Parlange, M. B., Bou-Zeid, E., Barrenetxea, G., et al., 2009. Estimation of urban sensible heat flux using a dense wireless network of observations, *Environmental Fluid Mechanics*, **9**, 635-653.

Nimmer, R. E., Osiensky, J. L., Binley, A. M., Sprenke, K. F., and Williams, B. C., 2007. Electrical resistivity imaging of conductive plume dilution in fractured rock, *Hydrogeology Journal*, **15**, 877-890.

Nimmer, R. E., Osiensky, J. L., Binley, A. M., and Williams, B. C., 2008. Three-dimensional effects causing artifacts in two-dimensional, cross-borehole, electrical imaging, *Journal of Hydrology*, **359**, 59-70.

Nyquist, J. E., Freyer, P. A., and Toran, L., 2008. Stream bottom resistivity tomography to map ground water discharge, *Ground Water*, **46**, 561-569.

Ogilvy, R. D., Meldrum, P. I., Kuras, O., Wilkinson, P. B., Chambers, J. E., et al., 2009. Automated monitoring of coastal aquifers with electrical resistivity tomography, *Near Surface Geophysics*, **7**, 367-375.

Oldenburg, D. W., and Li, Y. G., 1999. Estimating depth of investigation in dc resistivity and IP surveys, *Geophysics*, **64**, 403-416.

Olsson, O., Falk, L., Forslund, O., Lundmark, L., and Sandberg, E., 1992. Borehole radar applied to the characterization of hydraulically conductive fracture-zones in crystalline rock, *Geophysical Prospecting*, **40**, 109-142.

Oreskes, N., Shrader-Frechette, K., and Belitz, K., 1994. Verification, validation, and confirmation of numerical models in the earth sciences, *Science*, **263**, 641-646.

Orghidan, T., 1959. Ein neuer Lebensraum des unterirdischen Wassers: der hyporheische Biotop, *Arch. Hydrobiol.*, **55**, 392-414.

Osiensky, J. L., Nimmer, R., and Binley, A. M., 2004. Borehole cylindrical noise during hole-surface and hole-hole resistivity measurements, *Journal of Hydrology*, **289**, 78-94.

Paasche, H., Tronicke, J., Holliger, K., Green, A. G., and Maurer, H., 2006. Integration of diverse physical-property models: Subsurface zonation and petrophysical parameter estimation based on fuzzy c-means cluster analyses, *Geophysics*, **71**, H33-H44.

Paasche, H., and Tronicke, J., 2007. Cooperative inversion of 2D geophysical data sets: A zonal approach based on fuzzy c-means cluster analysis, *Geophysics*, **72**, A35-A39.

Paasche, H., Wendrich, A., Tronicke, J., and Trela, C., 2008. Detecting voids in masonry by cooperatively inverting P-wave and georadar traveltimes, *Journal of Geophysics and Engineering*, **5**, 256-267.

Paige, C. C., and Saunders, M. A., 1982. LSQR: An algorithm for sparse linear equations and sparse least squares, *ACM Transactions on Mathematical Software*, **8**, 43-71.

Palmer, M. A., Bernhardt, E. S., Allan, J. D., Lake, P. S., Alexander, G., et al., 2005. Standards for ecologically successful river restoration, *Journal of Applied Ecology*, **42**, 208-217.

Park, S. K., Johnston, M. J. S., Madden, T. R., Morgan, F. D., and Morrison, H. F., 1993. Electromagnetic precursors to earthquakes in the ULF band - a review of observations and mechanisms, *Reviews of Geophysics*, **31**, 117-132.

Parker, R. L., 1984. The inverse problem of resistivity sounding, *Geophysics*, **49**, 2143-2158.

Pasquale, N., Perona, P., Schneider, P., Shrestha, J., Wombacher, A., and Burlando, P., 2011. Modern comprehensive approach to monitor the morphodynamic evolution of a restored river corridor, *Hydrology and Earth System Sciences*, **15**, 1197-1212.

Perrier, F., and Morat, P., 2000. Characterization of electrical daily variations induced by capillary flow in the non-saturated zone, *Pure and Applied Geophysics*, **157**, 785-810.

Petiau, G., 2000. Second generation of lead-lead chloride electrodes for geophysical applications, *Pure and Applied Geophysics*, **157**, 357-382.

Podvin, P., and Lecomte, I., 1991. Finite difference computation of traveltimes in very contrasted velocity models: A massively parallel approach and its associated tools, *Geophysical Journal International*, **105**, 271-284.

Pollock, D., and Cirpka, O. A., 2010. Fully coupled hydrogeophysical inversion of synthetic salt tracer experiments, *Water Resources Research*, **46**, W07501.

Portniaguine, O., and Zhdanov, M. S., 1999. Focusing geophysical inversion images, *Geophysics*, **64**, 874-887.

Pratt, R. G., 1999. Seismic waveform inversion in the frequency domain, part 1: Theory and verification in a physical scale model, *Geophysics*, **64**, 888-901.

Pratt, R. G., and Shipp, R. M., 1999. Seismic waveform inversion in the frequency domain, part 2: Fault delineation in sediments using crosshole data, *Geophysics*, **64**, 902-914.

Pride, S., 1994. Governing equations for the coupled electromagnetics and acoustics of porous-media, *Physical Review B*, **50**, 15678-15696.

Pride, S. R., Berryman, J. G., and Harris, J. M., 2004. Seismic attenuation due to wave-induced flow, *Journal of Geophysical Research-Solid Earth*, **109**, B01201.

Pruess, K., Oldenburg, C. M., and Moridis, G. J., 1999. TOUGH2 user's guide version 2, Rep. LBNL--43134, 204 pp, Lawrence Berkeley National Laboratory.

Ptak, T., and Teutsch, G., 1994. Forced and natural gradient tracer tests in a highly heterogeneous porous aquifer - instrumentation and measurements, *Journal of Hydrology*, **159**, 79-104.

Ramirez, A., Daily, W., Labrecque, D., Owen, E., and Chesnut, D., 1993. Monitoring an underground steam injection process using electrical-resistance tomography, *Water Resources Research*, **29**, 73-87.

Ranguelova, E. B., 2002. *Segmentation of textured images on three-dimensional lattices*: PhD thesis, University of Dublin.

RECORD, 2011. Assessment and modeling of coupled ecological and hydrological dynamics in the restored corridor of the river, *Competence Center Environment and Sustainability*, http://www.cces.ethz.ch/projects/nature/Record.

Regli, C., Rauber, M., and Huggenberger, P., 2003. Analysis of aquifer heterogeneity within a well capture zone, comparison of model data with field experiments: A case study from the river Wiese, Switzerland, *Aquatic Sciences*, **65**, 111-128.

Revil, A., Cathles, L. M., Losh, S., and Nunn, J. A., 1998. Electrical conductivity in shaly sands with geophysical applications, *Journal of Geophysical Research - Solid Earth*, **103**, 23925-23936.

Revil, A., and Cathles, L. M., 1999. Permeability of shaly sands, *Water Resources Research*, **35**, 651-662.

Revil, A., Naudet, V., Nouzaret, J., and Pessel, M., 2003. Principles of electrography applied to self-potential electrokinetic sources and hydrogeological applications, *Water Resources Research*, **39**, 1114.

Revil, A., and Leroy, P., 2004. Constitutive equations for ionic transport in porous shales, *Journal of Geophysical Research-Solid Earth*, **109**, B03208.

Revil, A., and Linde, N., 2006. Chemico-electromechanical coupling in microporous media, *Journal of Colloid and Interface Science*, **302**, 682-694.

Revil, A., Linde, N., Cerepi, A., Jougnot, D., Matthai, S., and Finsterle, S., 2007. Electrokinetic coupling in unsaturated porous media, *Journal of Colloid and Interface Science*, **313**, 315-327.

Revil, A., Trolard, F., Bourrie, G., Castermant, J., Jardani, A., and Mendonca, C. A., 2009. Ionic contribution to the self-potential signals associated with a redox front, *Journal of Contaminant Hydrology*, **109**, 27-39.

Rizzo, E., Suski, B., Revil, A., Straface, S., and Troisi, S., 2004. Self-potential signals associated with pumping tests experiments, *Journal of Geophysical Research-Solid Earth*, **109**, B10203.

Robinson, D. A., Binley, A., Crook, N., Day-Lewis, F. D., Ferre, T. P. A., et al., 2008. Advancing process-based watershed hydrological research using near-surface geophysics: A vision for, and review of, electrical and magnetic geophysical methods, *Hydrological Processes*, **22**, 3604-3635.

Rubin, Y., and Hubbard, S. S. (Eds.), 2005. *Hydrogeophysics*, Springer, Dordrecht, The Netherlands.

Rücker, C., Günther, T., and Spitzer, K., 2006. Three-dimensional modelling and inversion of dc resistivity data incorporating topography - I. Modelling, *Geophysical Journal International*, **166**, 495-505.

Ruelleu, S., Moreau, F., Bour, O., Gapais, D., and Martelet, G., 2010. Impact of gently dipping discontinuities on basement aquifer recharge: An example from Ploemeur (Brittany, France), *Journal of Applied Geophysics*, **70**, 161-168.

Samaritani, E., Shrestha, J., Fournier, B., Frossard, E., Gillet, F., et al., 2011. Heterogeneity of soil carbon pools and fluxes in a channelized and a restored floodplain section (Thur River, Switzerland), *Hydrology and Earth System Sciences Discussions*, **8**, 1059-1091.

Sambridge, M., Braun, J., and Mcqueen, H., 1995. Geophysical parametrization and interpolation of irregular data using natural neighbors, *Geophysical Journal International*, **122**, 837-857.

Sandberg, S. K., Slater, L. D., and Versteeg, R., 2002. An integrated geophysical investigation of the hydrogeology of an anisotropic unconfined aquifer, *Journal of Hydrology*, **267**, 227-243.

Saracco, G., Labazuy, P., and Moreau, F., 2004. Localization of self-potential sources in volcano-electric effect with complex continuous wavelet transform and electrical tomography methods for an active volcano, *Geophysical Research Letters*, **31**, L12610.

Schälchli, U., 1992. The clogging of coarse gravel river beds by fine sediment, *Hydrobiologia*, **235-236**, 189-197.

Schälchli, U., 2008. Geschiebehaushalt im Thurgebiet, *Wasser Energie Luft*, **100**, 23-28.

Schäppi, B., Perona, P., Schneider, P., and Burlando, P., 2010. Integrating river cross section measurements with digital terrain models for improved flow modelling applications, *Computers & Geosciences*, **36**, 707-716.

Scheibe, T. D., and Chien, Y. J., 2003. An evaluation of conditioning data for solute transport prediction, *Ground Water*, **41**, 128-141.

Schmidt, C., Bayer-Raich, M., and Schirmer, M., 2006. Characterization of spatial heterogeneity of groundwater-stream water interactions using multiple depth streambed temperature measurements at the reach scale, *Hydrology and Earth System Sciences*, **10**, 849-859.

Schmidt, C., Conant, B., Bayer-Raich, M., and Schirmer, M., 2007. Evaluation and field-scale application of an analytical method to quantify groundwater discharge using mapped streambed temperatures, *Journal of Hydrology*, **347**, 292-307.

Schneider, P., Vogt, T., Schirmer, M., Doetsch, J., Linde, N., et al., 2011. Towards improved instrumentation for assessing river-groundwater interactions in a restored river corridor, *Hydrology and Earth System Sciences*, **15**, 2531-2549.

Schön, J. H., 1996. *Physical properties of rocks: Fundamentals and principles of petrophysics*, Elsevier Science Publishing Company, Inc.

Schulmeister, M. K., Butler, J. J., Healey, J. M., Zheng, L., Wysocki, D. A., and McCall, G. W., 2003. Direct-push electrical conductivity logging for high-resolution hydrostratigraphic characterization, *Ground Water Monitoring and Remediation*, **23**, 52-62.

Schwarzenbach, R. P., and Westall, J., 1981. Transport of non-polar organic-compounds from surface-water to groundwater - Laboratory sorption studies, *Environmental Science & Technology*, **15**, 1360-1367.

Schwarzenbach, R. P., Giger, W., Hoehn, E., and Schneider, J. K., 1983. Behavior of organic-compounds during infiltration of river water to groundwater - Field studies, *Environmental Science & Technology*, **17**, 472-479.

Schwarzenbach, R. P., Escher, B. I., Fenner, K., Hofstetter, T. B., Johnson, C. A., et al., 2006. The challenge of micropollutants in aquatic systems, *Science*, **313**, 1072-1077.

Seiz, G., and Foppa, N., 2007. Nationales Klima-Beobachtungssystem (GCOS Schweiz), *Bundesamt für Meteorologie und Klimatologie, MeteoSchweiz und ProClim, Bern, Switzerland*.

Selker, J. S., Thevenaz, L., Huwald, H., Mallet, A., Luxemburg, W., et al., 2006. Distributed fiber-optic temperature sensing for hydrologic systems, *Water Resources Research*, **42**, W12202.

Sen, P. N., Scala, C., and Cohen, M. H., 1981. A self-similar model for sedimentary-rocks with application to the dielectric-constant of fused glass-beads, *Geophysics*, **46**, 781-795.

Shankar, V., Eckert, P., Ojha, C. S. P., and Konig, C. M., 2009. Transient three-dimensional modeling of riverbank filtration at Grind well field, Germany, *Hydrogeology Journal*, **17**, 321-326.

Sheffer, M. R., and Oldenburg, D. W., 2007. Three-dimensional modelling of streaming potential, *Geophysical Journal International*, **169**, 839-848.

Sill, W. R., 1983. Self-potential modeling from primary flows, *Geophysics*, **48**, 76-86.

Silliman, S. E., and Booth, D. F., 1993. Analysis of time-series measurements of sediment temperature for identification of gaining vs losing portions of Juday-Creek, Indiana, *Journal of Hydrology*, **146**, 131-148.

Singha, K., and Gorelick, S. M., 2005. Saline tracer visualized with three-dimensional electrical resistivity tomography: Field-scale spatial moment analysis, *Water Resources Research*, **41**, W05023.

Sjödahl, P., Dahlin, T., and Johansson, S., 2009. Embankment dam seepage evaluation from resistivity monitoring data, *Near Surface Geophysics*, **7**, 463-474.

Slater, L., and Sandberg, S. K., 2000. Resistivity and induced polarization monitoring of salt transport under natural hydraulic gradients, *Geophysics*, **65**, 408-420.

Slater, L., Binley, A. M., Daily, W., and Johnson, R., 2000. Cross-hole electrical imaging of a controlled saline tracer injection, *Journal of Applied Geophysics*, **44**, 85-102.

Slater, L., and Binley, A., 2006. Synthetic and field-based electrical imaging of a zerovalent iron barrier: Implications for monitoring long-term barrier performance, *Geophysics*, **71**, B129-B137.

Slob, E., Sato, M., and Olhoeft, G., 2010. Surface and borehole ground-penetrating-radar developments, *Geophysics*, **75**, A103-A120.

Smith, D. G., and Jol, H. M., 1992. Ground-penetrating radar investigation of a Lake Bonneville delta, Provo level, Brigham City, Utah, *Geology*, **20**, 1083-1086.

Soar, P. J., and Thorne, C. R., 2001. *Channel restoration design for meandering rivers*, U.S. Army Engineer Research and Development Center, Vicksburg, Miss.

Spillmann, T., Maurer, H., Willenberg, H., Evans, K. F., Heincke, B., and Green, A. G., 2007. Characterization of an unstable rock mass based on borehole logs and diverse borehole radar data, *Journal of Applied Geophysics*, **61**, 16-38.

Springer, R. K., and Gelhar, L. W., 1991. Characterization of large-scale aquifer heterogeneity in glacial outwash by analysis of slug tests with oscillatory response, *US Geological Survey, Cape Cod*, Report 91-4034.

Stanford, J. A., and Ward, J. V., 1988. The hyporheic habitat of river ecosystems, *Nature*, **335**, 64-66.

Stanford, J. A., and Ward, J. V., 1993. An ecosystem perspective of alluvial rivers - connectivity and the hyporheic corridor, *Journal of the North American Benthological Society*, **12**, 48-60.

Stauffer, F., and Dracos, T., 1986. Experimental and numerical study of water and solute infiltration in layered porous-media, *Journal of Hydrology*, **84**, 9-34.

Storey, R. G., Howard, K. W. F., and Williams, D. D., 2003. Factors controlling riffle-scale hyporheic exchange flows and their seasonal changes in a gaining stream: A three-dimensional groundwater flow model, *Water Resources Research*, **39**, 1034.

Streich, R., van der Kruk, J., and Green, A. G., 2006. Three-dimensional multicomponent georadar imaging of sedimentary structures, *Near Surface Geophysics*, **4**, 39-48.

Streich, R., and van der Kruk, J., 2007a. Accurate imaging of multicomponent GPR data based on exact radiation patterns, *Ieee Transactions on Geoscience and Remote Sensing*, **45**, 93-103.

Streich, R., and van der Kruk, J., 2007b. Characterizing a GPR antenna system by near-field electric field measurements, *Geophysics*, **72**, A51-A55.

Stummer, P., Maurer, H., and Green, A. G., 2004. Experimental design: Electrical resistivity data sets that provide optimum subsurface information, *Geophysics*, **69**, 120-139.

Suski, B., Revil, A., Titov, K., Konosavsky, P., Voltz, M., et al., 2006. Monitoring of an infiltration experiment using the self-potential method, *Water Resources Research*, **42**, W08418.

SVGW, 2004. Jahrbuch 2003/2004, *SVGW, Zürich*.

SVGW, 2007. Empfehlungen – Revitalisierung im Einflussbereich von Trinkwasserfassungen, *Zürich, Switzerland*.

Talley, J., Baker, G. S., Becker, M. W., and Beyrle, N., 2005. Four dimensional mapping of tracer channelization in subhorizontal bedrock fractures using surface ground penetrating radar, *Geophysical Research Letters*, **32**, L04401.

Tarantola, A., 1984a. Inversion of seismic-reflection data in the acoustic approximation, *Geophysics*, **49**, 1259-1266.

Tarantola, A., 1984b. Linearized inversion of seismic-reflection data, *Geophysical Prospecting*, **32**, 998-1015.

Tarantola, A., 1986. A strategy for nonlinear elastic inversion of seismic-reflection data, *Geophysics*, **51**, 1893-1903.

Thony, J. L., Morat, P., Vachaud, G., and LeMouel, J. L., 1997. Field characterization of the relationship between electrical potential gradients and soil water flux, *Comptes Rendus De L'Academie Des Sciences*, **325**, 317-321.

Topp, G. C., Davis, J. L., and Annan, A. P., 1980. Electromagnetic determination of soil-water content - Measurements in coaxial transmission-lines, *Water Resources Research*, **16**, 574-582.

Topp, G. C., Davis, J. L., and Annan, A. P., 1982. Electromagnetic determination of soil-water content using TDR 2. Evaluation of installation and configuration of parallel transmission-lines, *Soil Science Society of America Journal*, **46**, 678-684.

Torrence, C., and Compo, G. P., 1998. A practical guide to wavelet analysis, *Bulletin of the American Meteorological Society*, **79**, 61-78.

Touchard, F., 1999. *Caractérisation hydrogéologique d'un aquifère en socle fracture. Site de Ploëmeur (Morbihan)*: PhD thesis, University of Rennes I.

Trefry, M. G., and Muffels, C., 2007. Feflow: A finite-element ground water flow and transport modeling tool, *Ground Water*, **45**, 525-528.

Triska, F. J., Kennedy, V. C., Avanzino, R. J., Zellweger, G. W., and Bencala, K. E., 1989. Retention and transport of nutrients in a 3rd-order stream in Northwestern California - hyporheic processes, *Ecology*, **70**, 1893-1905.

Triska, F. J., Duff, J. H., and Avanzino, R. J., 1993a. Patterns of hydrological exchange and nutrient transformation in the hyporheic zone of a gravel-bottom stream - examining terrestrial aquatic linkages, *Freshwater Biology*, **29**, 259-274.

Triska, F. J., Duff, J. H., and Avanzino, R. J., 1993b. The role of water exchange between a stream channel and its hyporheic zone in nitrogen cycling at the terrestrial aquatic interface, *Hydrobiologia*, **251**, 167-184.

Tronicke, J., Dietrich, P., Wahlig, U., and Appel, E., 2002. Integrating surface georadar and crosshole radar tomography: A validation experiment in braided stream deposits, *Geophysics*, **67**, 1516-1523.

Tronicke, J., and Holliger, K., 2004. Effects of gas- and water-filled boreholes on the amplitudes of crosshole georadar data as inferred from experimental evidence, *Geophysics*, **69**, 1255-1260.

Tronicke, J., Holliger, K., Barrash, W., and Knoll, M. D., 2004. Multivariate analysis of cross-hole georadar velocity and attenuation tomograms for aquifer zonation, *Water Resources Research*, **40**, W01519.

Trubilowicz, J., Cai, K., and Weiler, M., 2009. Viability of motes for hydrological measurement, *Water Resources Research*, **45**, W00D22.

Trush, W. J., McBain, S. M., and Leopold, L. B., 2000. Attributes of an alluvial river and their relation to water policy and management, *Proceedings of the National Academy of Sciences of the United States of America*, **97**, 11858-11863.

Tryggvason, A., Rögnvaldsson, S. T., and Flóvenz, Ó. G., 2002. Three-dimensional imaging of the P- and S-wave velocity structure and earthquake locations beneath Southwest Iceland, *Geophysical Journal International*, **151**, 848-866.

Tryggvason, A., and Linde, N., 2006. Local earthquake (LE) tomography with joint inversion for P- and S-wave velocities using structural constraints, *Geophysical Research Letters*, **33**, L07303.

Tryggvason, A., and Bergman, B., 2006. A traveltime reciprocity discrepancy in the Podvin & Lecomte time3d finite difference algorithm, *Geophysical Journal International*, **165**, 432-435.

Tsoflias, G. P., Halihan, T., and Sharp, J. M., 2001. Monitoring pumping test response in a fractured aquifer using ground-penetrating radar, *Water Resources Research*, **37**, 1221-1229.

Tsoflias, G. P., and Becker, M. W., 2008. Ground-penetrating-radar response to fracture-fluid salinity: Why lower frequencies are favorable for resolving salinity changes, *Geophysics*, **73**, J25-J30.

Tubino, M., and Seminara, G., 1990. Free forced interactions in developing meanders and suppression of free bars, *Journal of Fluid Mechanics*, **214**, 131-159.

Tufenkji, N., Ryan, J. N., and Elimelech, M., 2002. The promise of bank filtration, *Environmental Science & Technology*, **36**, 422A-428A.

Turesson, A., 2006. Water content and porosity estimated from ground-penetrating radar and resistivity, *Journal of Applied Geophysics*, **58**, 99-111.

van Genuchten, M. T., 1980. A closed-form equation for predicting the hydraulic conductivity of unsaturated soils, *Soil Science Society of America Journal*, **44**, 892-898.

Vasco, D. W., Peterson, J. E., and Majer, E. L., 1995. Beyond ray tomography - Wavepaths and fresnel volumes, *Geophysics*, **60**, 1790-1804.

Vereecken, H., Binley, A., Cassiani, G., Revil, A., and Titov, K. (Eds.), 2006. *Applied hydrogeophysics*, Springer, Dordrecht, The Netherlands.

Vereecken, H., Huisman, J. A., Bogena, H., Vanderborght, J., Vrugt, J. A., and Hopmans, J. W., 2008. On the value of soil moisture measurements in vadose zone hydrology: A review, *Water Resources Research*, **44**, W00D06.

Vogt, T., Hoehn, E., Schneider, P., and Cirpka, O. A., 2009. Untersuchung der Flusswasserinfiltration in voralpinen Schottern mittels Zeitreihenanalyse, *Grundwasser*, **14**, 179-194.

Vogt, T., Schneider, P., Hahn-Woernle, L., and Cirpka, O. A., 2010a. Estimation of seepage rates in a losing stream by means of fiber-optic high-resolution vertical temperature profiling, *Journal of Hydrology*, **380**, 154-164.

Vogt, T., Hoehn, E., Schneider, P., Freund, A., Schirmer, M., and Cirpka, O. A., 2010b. Fluctuations of electrical conductivity as a natural tracer for bank filtration in a losing stream, *Advances in Water Resources*, **33**, 1296-1308.

von Gunten, H. R., Karametaxas, G., and Keil, R., 1994. Chemical Processes in Infiltrated Riverbed Sediments, *Environmental Science & Technology*, **28**, 2087-2093.

von Gunten, U., and Zobrist, J., 1993. Biogeochemical changes in groundwater-infiltration systems - column studies, *Geochimica Et Cosmochimica Acta*, **57**, 3895-3906.

Vozoff, K., and Jupp, D. L. B., 1975. Joint inversion of geophysical data, *Geophysical Journal of the Royal Astronomical Society*, **42**, 977-991.

Ward, A. S., Gooseff, M. N., and Singha, K., 2010. Imaging hyporheic zone solute transport using electrical resistivity, *Hydrological Processes*, **24**, 948-953.

Ward, J. V., 1989. The four-dimensional nature of lotic ecosystems, *Journal of the North American Benthological Society*, **8**, 2-8.

Watanabe, T., Nihei, K. T., Nakagawa, S., and Myer, L. R., 2004. Viscoacoustic wave form inversion of transmission data for velocity and attenuation, *Journal of the Acoustical Society of America*, **115**, 3059-3067.

Waxman, M. H., and Smits, L. J. M., 1968. Electrical Conductivities in Oil-Bearing Shaly Sands, *Society of Petroleum Engineers Journal*, **8**, 107.

West, L. J., Handley, K., Huang, Y., and Pokar, M., 2003. Radar frequency dielectric dispersion in sandstone: Implications for determination of moisture and clay content, *Water Resources Research*, **39**, 1026.

Western, A. W., Grayson, R. B., and Blöschl, G., 2002. Scaling of soil moisture: A hydrologic perspective, *Annual Review of Earth and Planetary Sciences*, **30**, 149-180.

Wilkinson, P. B., Meldrum, P. I., Kuras, O., Chambers, J. E., Holyoake, S. J., and Ogilvy, R. D., 2010. High-resolution electrical resistivity tomography monitoring of a tracer test in a confined aquifer, *Journal of Applied Geophysics*, **70**, 268-276.

Winship, P., Binley, A., and Gomez, D., 2006. Flow and transport in the unsaturated Sherwood Sandstone: Characterization using cross-borehole geophysical methods, *Fluid Flow and Solute Movement in Sandstones: The Onshore UK Permo-Triassic Red Bed Sequence*, **263**, 219-231.

Wishart, D. N., Slater, L. D., and Gates, A. E., 2006. Self potential improves characterization of hydraulically-active fractures from azimuthal geoelectrical measurements, *Geophysical Research Letters*, **33**, L17314.

Woessner, W. W., 2000. Stream and fluvial plain ground water interactions: Rescaling hydrogeologic thought, *Ground Water*, **38**, 423-429.

Wombacher, A., and Schneider, P., 2010. Observation centric sensor data model, *Technical Report TR-CTIT-10-13, University of Twente, Enschede*, ISSN 1381-3625.

Woolsey, S., Capelli, F., Gonser, T., Hoehn, E., Hostmann, M., et al., 2007. A strategy to assess river restoration success, *Freshwater Biology*, **52**, 752-769.

Worthington, P. F., 1993. The uses and abuses of the archie equations 1. The formation factor porosity relationship, *Journal of Applied Geophysics*, **30**, 215-228.

Wriedt, G., and Rode, M., 2006. Modelling nitrate transport and turnover in a lowland catchment system, *Journal of Hydrology*, **328**, 157-176.

Wroblicky, G. J., Campana, M. E., Valett, H. M., and Dahm, C. N., 1998. Seasonal variation in surface-subsurface water exchange and lateral hyporheic area of two stream-aquifer systems, *Water Resources Research*, **34**, 317-328.

Yeh, T. C. J., Liu, S., Glass, R. J., Baker, K., Brainard, J. R., et al., 2002. A geostatistically based inverse model for electrical resistivity surveys and its applications to vadose zone hydrology, *Water Resources Research*, **38**, 1278.

Yeh, T. C. J., Lee, C. H., Hsu, K. C., Illman, W. A., Barrash, W., et al., 2008. A view toward the future of subsurface characterization: CAT scanning groundwater basins, *Water Resources Research*, **44**, W03301.

Yilmaz, Ö., 2001. *Seismic data processing*, Society of Exploration Geophysicists, Tulsa, USA.

Zhang, J., and Morgan, F. D., 1997. Joint Seismic and Electrical Tomography, *Proceedings of the Symposium on the Application of Geophysics to Engineering and Environmental Problems*, 391-396.

Zhdanov, M. S., 2009. New advances in regularized inversion of gravity and electromagnetic data, *Geophysical Prospecting*, **57**, 463-478.

Zhou, B., and Greenhalgh, S. A., 2003. Crosshole seismic inversion with normalized full-waveform amplitude data, *Geophysics*, **68**, 1320-1330.

Zonge, K., Wynn, J., and Urquhart, S., 2005. Resistivity, induced polarization, and complex resistivity, in *Near Surface Geophysics*, edited by D. K. Butler, pp. 265-300, SEG.

Zurbuchen, B. R., Zlotnik, V. A., and Butler, J. J., 2002. Dynamic interpretation of slug tests in highly permeable aquifers, *Water Resources Research*, **38**, 1025.